REPORT NO.
EERC 72–5
OCTOBER 1972

EARTHQUAKE ENGINEERING RESEARCH CENTER

CYCLIC BEHAVIOR OF THREE R.C. FLEXURAL MEMBERS WITH HIGH SHEAR

by
E. P. POPOV
V. V. BERTERO
H. KRAWINKLER

Report to
National Science Foundation

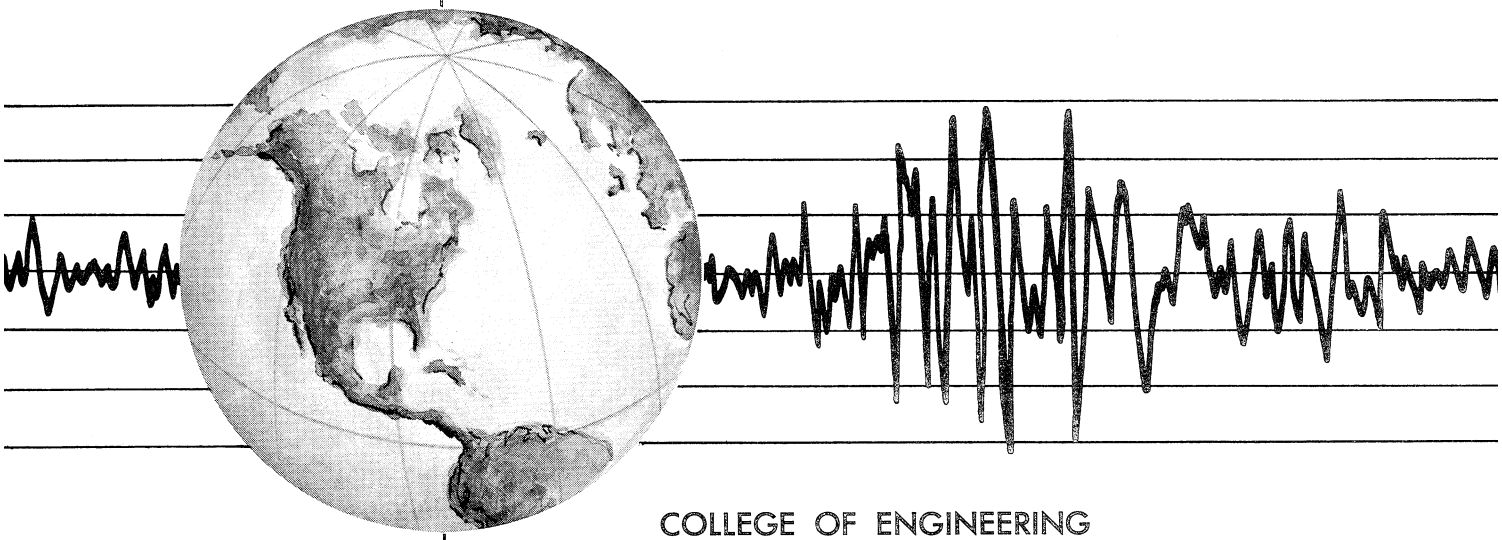

COLLEGE OF ENGINEERING
UNIVERSITY OF CALIFORNIA · Berkeley, California

CYCLIC BEHAVIOR OF THREE REINFORCED CONCRETE FLEXURAL MEMBERS WITH HIGH SHEAR

by

EGOR P. POPOV
Professor of Civil Engineering

VITELMO V. BERTERO
Professor of Civil Engineering

HELMUT KRAWINKLER
Assistant Research Engineer

in collaboration with

R. ALAMO-NEIDHART

G. ELIAS

M. MA

Graduate Students

Report to
National Science Foundation

EARTHQUAKE ENGINEERING RESEARCH CENTER

College of Engineering
University of California
Berkeley, California

October 1972

ABSTRACT

The behavior of three large reinforced concrete cantilever beams is discussed in this report. The beams were 15 in. by 29 in. in cross-section and all had six #9 deformed bars for longitudinal reinforcement at the top and bottom. The shear reinforcement differed in size and spacing for each specimen. With heavy longitudinal reinforcement and small cantilever length (78 in.), high shearing forces were transmitted simultaneously with the bending moments.

The principal objective of this investigation was to study the effects of the high shear forces on deformation, strength, stiffness and energy dissipation capacity of flexural members. The nominal shear stress at ultimate load was approximately equal to $6\sqrt{f'_c}$ for all three specimens. The specimens failed in shear; and in the post-yielding range shear-type deformations contributed significantly to the tip deflection of the cantilevers. These shear-type deformations led to a deterioration of the initial loading stiffness and consequently to a pronounced pinching of the hysteresis loops. The experiments showed that repeated reversed loading of flexural members leads to a deterioration in shear resistance. If the shear forces are high, this deterioration may lead to a shear failure at rather low flexural ductilities. For earthquake resistant design, a reevaluation of the current ACI Code (1971) design equations for shear reinforcement (Section 11.6) seems therefore necessary.

ACKNOWLEDGEMENTS

The work reported here originated from the research projects of two graduate students. The first one, consisting of experiments with Beams 35 and 46, was completed by Mr. R. Alamo-Neidhart in the Fall of 1970. The second, consisting of the experiment with Beam 43, was completed by Mr. G. Elias in the Summer of 1971. The testing fixture used was originally developed in connection with similar work on an AISI project on large steel beams. Funds for the purchase of the materials used were from a donation by John A. Blume to EERC. The University provided the necessary shop support. Another graduate student, Mr. S. Ma, assisted with the data reduction. Ann Marie Berlin assisted with editing of the report, the typing was done by Shirley Edwards. NSF provided the financial support for preparation of the report in its present form.

The authors are most grateful for the various financial support given this project, as well as for the conscientious work of the graduate students.

As the information on the behavior of large reinforced concrete beams with high shear under cyclic loading is very limited at the present time, it is hoped that this report will be found useful by the designers of earthquake resistant structures.

TABLE OF CONTENTS

NOTATION

A_s	area of tension reinforcement
A'_s	area of compression reinforcement
b	width of beam
d	distance from extreme compression fiber to centroid of tension reinforcement
d'	distance from extreme compression fiber to centroid of compression reinforcement
f'_c	compressive strength of concrete
f_{max}	maximum strength of reinforcement
f_t	modulus of rupture of concrete
f_y	yield strength of reinforcement
h	height of beam
ℓ	length of beam
M_c	moment at diagonal tension cracking
M_{cr}	moment at flexural cracking
M_{max}	maximum moment in cantilever (from experiment)
M_u	ultimate moment (computed)
M_{wl}	moment at working stress level
M_y	moment at yielding of main reinforcement
P	applied load
p	A_s/bd = ratio of area of tension reinforcement to effective area of concrete
p'	A'_s/bd = ratio of area of compression reinforcement to effective area of concrete

p_b reinforcement ratio producing balanced conditions

v V/bd = nominal shear stress

V_c shear at diagonal tension cracking

V_{cr} shear at flexural cracking

V_{max} maximum shear in cantilever (from experiment)

V_s shear carried by web reinforcement

V_u shear at ultimate moment ($V_u = M_u/\ell$)

V_{ult} computed shear capacity ($V_{ult} = V_s + V_c$)

V_{wl} shear at working stress level

V_y shear at yielding of main reinforcement

δ_{max} maximum tip deflection

δ_y tip deflection at yield

θ_{FE} fixed end rotation

θ_{pl} plastic rotation at critical region

μ ductility factor

Φ curvature

1. INTRODUCTION

1.1 Nature of the Problem

Economic considerations require that in most building structures which are likely to be subjected to severe earthquakes some inelastic deformations in the structural members must be tolerated [1]. For this reason, for the last decade earthquake engineering research has been directed towards establishing design criteria that consider the postelastic behavior of structural members and systems. Moreover, since the response of a structure to earthquakes is a dynamic rather than a static problem, the capability of a structure to absorb and ultimately dissipate energy becomes the governing design criterion. This energy absorption capability of a structure depends on its strength and ductility as well as on its ability to resist repeated and reversed loadings.

During a severe earthquake a large portion of the energy imparted to the structure by the ground motion has to be absorbed and dissipated by inelastic deformations in the structural elements. However, in conventional engineering practice, the design of structural members is based largely on elastic stiffness and on resistance to monotonically increasing loads. For instance, in ultimate strength design, flexural members are designed to develop an ultimate moment capacity, M_u, and a sufficient amount of shear reinforcement is provided to prevent failure in shear before M_u is attained. A certain ductility of members is assured implicitly by establishing upper and lower bounds on the reinforcement ratio p [2, 3] and by requiring a certain amount and spacing of lateral reinforcement.

Experimental studies of the behavior of flexural members under repeated reversed loading have been carried out by various investigators [4-8]. However, no general rules have been established yet to construct adequate mechanical models and to define safe values of the rotation capacity for critical flexural regions subjected to load reversals, especially under high shear forces.

At present it is recognized that due to the considerable uncertainties involved in earthquake-resistant design it is advantageous to provide the structure with high ductility. Usually adequate ductility can be achieved at a reasonable cost by carefully detailing the critical regions. To obtain high ductility in reinforced concrete flexural members, it is necessary to avoid or delay the inelastic buckling of the main reinforcing and to pay particular attention to the proper design of shear reinforcement to avoid brittle failure due to diagonal tension.

Experimental studies of beams in pure bending and in bending with small shear [4] indicate that in general the curvature and rotation ductilities under cyclic loadings exceed those under monotonic loading. This is not necessarily true when bending is accompanied by high shear. Then the problem is how much shear reinforcement has to be provided to assure sufficient rotation capacity, ductility, in the beam. Hence the effects of load reversals on the shear resistance of reinforced concrete beams and the effects of shear deformations on the stiffness deterioration of flexural members under load reversals need to be studied.

A research program of both analytical and experimental studies has been initiated at the University of California, Berkeley, to investigate these problems. The goal of this investigation is

twofold. First, for design purposes, to arrive at design criteria that would prevent premature failure either in flexure or shear so that a given amount of energy could be absorbed and dissipated in the member. Second, for analysis purposes, to predict realistically the moment-curvature relationship of flexural members for arbitrary loading. Such a prediction would have to include stiffness deterioration and the effects of shear on strength and on deformational and energy dissipation capacities.

1.2 Objective and Scope

The primary objective of the investigation reported herein was to obtain information on the strength, ductility, and energy absorption and dissipation characteristics of reinforced concrete regions subjected to severe cycles of bending moment reversals and high shear forces. Emphasis was placed on the influence of the size and spacing of web reinforcement.

To achieve the objective, three large reinforced concrete cantilever beams were tested. The three beams had the same amount of main longitudinal reinforcement but each had different web reinforcement. The beams were subjected to alternating cyclic loading with varying magnitudes of peak loads or deformations chosen according to a preselected loading history. The present report gives details of the experiments carried out on the three beams and evaluates and discusses the significance of the results obtained.

2. TEST SPECIMENS

2.1 Description of Test Specimens

The type of specimen selected for the experimental investigation is shown in Fig. 1. It consists of a 78 in. long cantilever beam having a cross section of 15 x 29 inches. The shear span to effective depth ratio, ℓ/d, is equal to 3.1, and since $\ell/d > 2.5$ these beams are considered "normal beams" [9].

All three specimens were reinforced longitudinally with six #9 deformed bars on top and bottom with $p = p' = 0.0158$. The major variable was the size and the spacing of the web reinforcement, which consists of stirrup-ties. On this basis the specimens were designated by two digits, the first digit defining the size of the ties and the second their spacing. Table 1 summarizes the reinforcement used in each of the beams.

2.2 Characteristics of Materials

The main mechanical characteristics of the materials are also summarized in Table 1, and detailed information on the material properties is given in Appendix A. It should be noted that the ultimate concrete strength, f'_c, was approximately the same for the first two specimens (3860 psi and 3990 psi) at the time of testing but was about 25 percent higher for the third specimen (5030 psi). It was necessary to increase concrete strength of the third specimen to conform to the ACI 1971 Code, which requires in seismic design that the maximum reinforcement ratio for flexural members should not exceed 0.50 of the ratio producing balanced conditions [Ref. 2, Section A.5.1].

The stress-strain diagrams for the main reinforcement #9 bars are shown in Fig. A2 in Appendix A. The computed moment capacities as shown in Table 2 are based on the actual yield strength f_y and when applicable, on the maximum steel strength f_{max}, which is about 55 percent higher than the yield strength.

2.3 Design of Web Reinforcement

As it was intended to vary the web reinforcement in the three specimens, different criteria were used for the design of the stirrup-ties. Beam 35 was designed according to the ACI 1963 Code [10], which assumes that concrete and web reinforcement participate in resisting the shear according to the ultimate design moment M_u as computed from Eq. 16.1 in the ACI 1963 Code. In Beam 46 it was assumed that concrete does not participate in carrying shear and that the full shear has to be taken by the web reinforcement. Similarly, in Beam 43 the contribution of the concrete to the shear resistance was assumed negligible, but the stirrup-ties were designed to resist the maximum shear that could be developed. This shear in turn corresponds to the maximum possible bending moment that can be produced at the root of the beam. This moment can be computed from the following equation [1]:

$$M_u = A'_s f'_{su} (d - d') + (A_s f_{su} - A'_s f'_{su})(d - d' - 0.4k''_u)$$

Since $p = p'$, the M_u can be obtained by assuming that only the main reinforcement participates in carrying moment and that both tension and compression reinforcement reach the actual maximum steel strength f_{max} obtained from tension tests on specimens of the reinforcing bars.

Hence

$$M_u = A'_s f_{max} (d - d').$$

The M_u obtained in this manner is an upper bound of the moment capacity, and consequently of the corresponding shear. Closely spaced stirrup-ties are required to resist this shear.

The predicted shear and moment capacities of the three test specimens are listed in Table 2. Numerical computations for the design of the beams are presented in detail in Appendix B.

2.4 Fabrication of Specimens

The formwork and reinforcement for a typical test specimen is shown in Fig. 2, and details of its fabrication are given in Appendix A. As can be seen from the photo in Fig. 2, the fixed end of the cantilever was built into a reinforced concrete column stub anchored to a reaction frame. This column stub was 90 in. long and had a square cross section of 18 in. by 18 in. Four #9 bars, with a clearance of 2.5 in. from the face toward the beam, were used as reinforcement for the column. For Beam 43 six additional #9 bars, 72 in. long, were added to provide additional strength to the connecting zone.

The longitudinal beam reinforcement was welded at the fixed end of the cantilever to the T-beam anchorage by means of connecting plates (see Fig. 1). In this manner the reinforcement was safely anchored, however, due to bond deterioration some slippage of the rebars in the connecting zone did occur. This slippage caused a fixed end rotation which did contribute to the recorded deflection at the tip of the cantilever.

3. EXPERIMENTAL SETUP AND TEST PROCEDURE

3.1 Loading Apparatus

To take advantage of an existing large capacity double-acting hydraulic actuator [11, 12], it was necessary to test the full-size cantilever beams in a horizontal position. The loading apparatus which is shown schematically in Fig. 3, consists of a loading reaction fixture with a hydraulic actuator mounted on it, a lateral guide frame, and a beam reaction fixture. The reaction fixtures are anchored to the test floor by means of prestressing rods.

For Beams 35 and 46, pieces of a W 18 x 50 beam, cut out as shown in Fig. 2, were partially embedded in the free end of the cantilevers. The force from the hydraulic actuator was transferred to the beam by means of a pin passed through the reinforced web of the steel piece. For Beam 43, a piece of W 24 x 76 was used in a similar manner. The actuator used was a Miller Model H hydraulic cylinder with a 14 in. bore and a 12 in. stroke, capable of developing a force of approximately 460 kips when operated at a pressure of 3000 psi. The loading ram of the actuator was strain gaged and calibrated to act as a transducer. The hydraulic power was supplied by the in-house hydraulic pumping system capable of producing 320 gollon per minute at 3000 psi pressure. An electro-hydraulic system employing a 30 gpm solenoid valve and an electronic switching unit was used to regulate the pressure in the hydraulic actuator.

3.2 Specimen Instrumentation

The deformations measured during the tests were the deflection of the cantilever tip, and the average curvatures in two regions adjacent

to the fixed end of the cantilever. The tip deflections were measured by means of a linear potentiometer attached to the ends of the beams. The average curvatures were measured with clip gages and linear potentiometers attached to aluminum yokes fixed to the concrete beams at distances of 6 in. and 17.25 in. from the fixed end of the cantilever. Curvatures were also obtained from reading dial gages attached to rods imbedded in the concrete at distances of 14.5 in. and 29 in. from the fixed end of the cantilevers.

The output from the linear potentiometers and the electrical resistance gages mounted on clip gages was fed into the Y channels of X-Y and X-Y-Y' recorders. The X channels recorded the applied load P, and thus continuous records of the load-deflection and load-curvature response of the specimens were obtained.

For Beam 46 two arch gages recorded continuously on an X-Y-Y' recorder the average strain over a 6 in. gage length in two reinforcing bars at the fixed end of the cantilever. Short rods were to be silver soldered to the reinforcing bars to attach these gages. Because of a fabrication error, the rods were welded and stress concentrations caused by this welding contributed to the premature fracture of the reinforcing steel at a strain of about 0.023 in./in.

All three specimens were whitewashed to make cracks in the concrete more visible; and, as the cracks appeared, they were marked and numbered sequentially to keep track of the history of cracking. The location of longitudinal and shear reinforcement was marked with felt-tip pen lines on the whitewash. These grid lines proved to be very useful in later stages of the experiments for measuring deformations across diagonal cracks.

Details of the instrumentation at the fixed end of the cantilever are shown in Fig. 4.

3.3 Test Procedure

Since one of the main purposes of the test program was to compare the relative performance of the specimens, the loading sequence was kept similar in each of the experiments. In the early stage of loading before the reinforcement yielded,loading was controlled by the magnitude of the load applied. Two complete load cycles were carried out at each loading step. The step sizes were determined by the appearance of the first flexural cracks, the first diagonal tension cracks and the initial yielding of the reinforcement.

After the reinforcement yielded,loading was controlled by the magnitude of the measured tip deflection. Two complete cycles were carried out at each selected value of deflection ductility. In this manner a family of progressively increasing loops was generated. The second cycle of each step size provided a measure of deterioration in stiffness and energy dissipation for successive similar cycles. The tip deflection was increased progressively until the specimens failed. The load was kept constant for a short period of time at points of load reversals to read the instruments and mark the cracks in the concrete.

It is recognized that the selected loading/deformation program might be far from representing the actual history of deformations the critical regions might undergo in case of real excitation. For each different type of structure and/or ground motion, a different loading/deformation response has to be expected. However, it is believed that

under the presence of high shear stepwise increasing deformation cycles form one of the most critical loading paths for assessing the strength, deformation, and energy dissipation capacities of flexural members.

4. EXPERIMENTAL RESULTS

4.1 General Behavior and Failure Modes

The peak loads and peak deflections of each cycle of the loading programs applied to the three test specimens are illustrated in Figs. 5-7. The service or working loads P_{wl}, the observed yield loads P_y, and yield deflections δ_y are noted on the diagrams. The post-yield strength and deflection ductility of the specimens can be obtained readily from these figures. Numerical values of the loads and deflections at significant points in the loading history are listed in Table 3. Hysteresis diagrams of the response of the three specimens are shown in Figs. 11-17.

These are some observations from the experiments:

1) Flexural cracks in each of the three beams were first observed at loads of approximately 20 kips. At this load an instantaneous drop in stiffness to about half the value before cracking can be detected from the continuous records (Fig. 11). The spacing of the flexural cracks was nearly uniform and approximately equal to 6 in. in all three specimens (Fig. 9).

2) Diagonal tension cracks were first observed at loads of about 50 to 60 kips and led to a further decrease in beam stiffness (Fig. 11). These cracks were extensions of the previously observed

flexural cracks. Load reversals beyond the load level at which the diagonal tension cracks occurred produced a diagonal grid of cracks crossing each other at approximately right angles (Figs. 8 and 9).

3) The tension reinforcement started to yield at moments 8 percent higher for Beams 35 and 46 and 16 percent higher for Beam 43 than that predicted by the ACI 1963 Code equations for the ultimate moment, using the actual yielding strength of the main reinforcement. The load-deflection and moment-curvature diagrams clearly show a yield plateau at this level of loading

4) Flexural and diagonal tension crack patterns were very similar in either direction of loading.

5) After several large displacement cycles, a relative movement of the rectangular concrete blocks between the grid of diagonal tension cracks occured, and the concrete cover all around the critical regions came loose.

6) Before the specimens failed, one or two main diagonal tension cracks opened up; the transverse displacement across these cracks on the concrete surface was as much as 2 in. (Fig. 8).

7) In all three specimens the main diagonal tension cracks ended at the root of the cantilevers at the level of the compression reinforcement.

8) Beams 35 and 43 failed in shear. Figure 8 show the two main diagonal cracks that caused the final failure of Beam 35. It can be seen from this photo taken after two cycles at maximum displacement that a significant portion of the cantilever tip deflection was caused by deformations across the cracks and not by flexural deformations.

Figure 10 shows the fixed end of Beam 43 after the test with the concrete core exposed. It can be observed that the diagonal tension cracks for this specimen are inclined at an angle substantially steeper than 45 degrees. The concrete surrounding the core came off without effort; and the concrete within the core was severely crumbled and offered little resistance. Note the deformation of the longitudinal reinforcement caused by dowel action.

9) Large diagonal cracks developed in Beam 46 (Fig. 9); but the actual failure, which occurred right at the face of the column stub, was caused by premature fracture of the longitudinal reinforcing bar to which the legs of one of the arch gages were welded. We believe that this specimen could have withstood more loading cycles without significantly deteriorating in strength if the steel had not failed.

4.2 P-δ Diagrams

The primary variables recorded continuously were the applied load P and the cantilever tip deflection δ. The measured deflection is the result of flexural and shear deformations in the beam and the fixed-end rotation caused by slippage of the reinforcement within the column stub. During the last few cycles before failure, the deflection δ increased significantly by shear displacements across the diagonal tension cracks. This is clearly indicated by the discontinuities in the grid lines marked on the specimens as illustrated in Fig. 8. Load-deflection diagrams are shown in Figs. 11-14. The first cycle of each loading step is drawn with solid lines and the second with dashed lines.

Figure 11 illustrates the behavior of Beam 46 in the early stages of loading. Three distinctly different stiffnesses can be

observed, one before flexural cracking (K_1), one before diagonal tension cracking (K_2) and one after that (K_3).

Figures 12-14 show the complete load-deflection history of the three specimens. The following observations can be made from these figures.

1) The load-deformation response is similar in both directions of loading.

2) There is no significant drop in flexural capacity during the repeated second cycle at each displacement amplitude prior to failure.

3) Two kinds of hystersis loops can be distinguished. Before shear deformations become pronounced, the loops are spindle shaped. A typical example is the loop drawn with solid lines from point 16 to 18 and back to 16a in Fig. 12. When shear deformations become prominent the loops take on a pinched shape, as demonstrated in the loop drawn with dashed lines from point 16a to 18a to 20 in Fig. 12 and in the large displacement loops in Fig. 14. The reason for this pinching is that at zero load the flexural and diagonal tension cracks are open and at reloading most of the shear has to be taken by dowel action. This leads to large shear deformations and consequently to a small initial loading stiffness. It is only when the cracks close and the "truss" formed by the confined concrete and the stirrup-ties starts to take shear, that stiffness increases again. From then on the stiffness is mainly determined by the flexural characteristics of the critical region.

4.3 M-Φ Diagrams

The average values of the beam curvature were measured over a length of 6 in. and 11.25 in., close to the fixed end of the cantilever. In Fig. 1, the points where the yokes are attached to the beam are marked with crosses on the near face. Four additional points are on the other side of the beam. For the uncracked beam the measured values of the displacement between the yokes provide accurate information on flexural deformations. If diagonal tension cracks develop in the beam, measurements may include relative rotation due to displacements across the cracks. Hence the M-Φ diagrams have to be interpreted with caution, and the crack pattern has to be considered in the interpretation. It has to be emphasized that the average curvatures measured in the 6 in. region at the fixed end of the cantilever include the fixed-end rotation (θ_{FE}) due to slippage of the rebars in the anchored zone, since the linear potentiometers were attached to the concrete face of the column stubs and not to the ideal fixed end of the cantilevers. The recorded curvature is therefore denoted $\bar{\Phi}_1$, but the actual average curvature is:

$$\Phi_1 = \bar{\Phi}_1 - \frac{\theta_{FE}}{6.00}$$

Unfortunately, it was not possible to measure θ_{FE} with the instrumentation available.

The M-Φ diagrams for the three specimens are shown in Figs. 15-17. These figures show a wide variation in the curvature distribution among the three test specimens. Since all three specimens have the same amount of longitudinal reinforcement, this variation can

be attributed to the difference in crack patterns. As has already been pointed out by Bertero and Felippe [13], the curvatures are strongly dependent on the degree of confinement of the concrete core, i.e., on the amount of web reinforcement, since inelastic deformations spread further with increasing confinement. Also the location of the main diagonal tension cracks, which affect flexural deformations, have a significant influence on the recorded average curvature distribution.

The variation of the average curvature close to the fixed end of the cantilever is shown in Fig. 18 for several points in the loading history of the three specimens. The presented graph clearly illustrates the difference in the curvature distribution between the first two specimens (Beams 35 and 46) and Beam 43, which is heavily reinforced with vertical stirrups.

4.4 Strain in Reinforcing Steel

The average strain in two reinforcing bars over a gage length of 6 in. at the fixed end of Beam 46 is shown in Fig. 19. When compared with Fig. 16, it can be seen that curvature and steel strain are not at all similar. While Fig. 16 indicates a change of sign in curvature, the strains in the reinforcing bars in Fig. 19 remain of the same sign except for the first loading beyond yield when compression reinforcement shows a small compressive strain.

The maximum average tensile strain recorded in the reinforcement of Beam 46 was 2.4 percent, which was far below the ultimate strain of the steel. In this specimen a 0.5 in. diameter rod was spot welded to a 1.12 in. diameter bar; and since the reinforcing bar failed at this low level of strain, it is clear that welding can have a highly detrimental effect on the material properties of steel.

5. DISCUSSION OF TEST RESULTS

5.1 Moment Capacity

An inspection of Figs. 12-17 shows that the envelopes of the load-deflection and moment-curvature relationships can be approximated by an elastic stiffness of the cracked section followed by a strain hardening stiffness. In earthquake-resistant design in which energy absorption and dissipation are the governing criteria, the increase in strength due to strain hardening (magnitude of the strain hardening stiffness) is usually not of foremost importance. The main problems here are the deterioration of stiffness under load reversals and the determination of a "useful limit" of deformation beyond which no reliance can be placed upon the energy absorption characteristics of the structural member. This useful limit of deformation depends again on the history of deformation in the critical regions.

Previous investigations [4] have shown that flexural members subjected to pure bending or bending with low shear exhibit very high ductilities under load reversals, provided that buckling of the compression reinforcement is prevented. Furthermore, load reversals appear to benefit the flexural capacity even at very high ductilities if these load reversals are applied with a gradually increasing displacement amplitude. In this case, the behavior of flexural members after severe cyclic loading in the inelastic range is determined by the mechanical characteristics of the steel. This is a consequence of the bond deterioration that occurs between main cracks as the reversals of moments increase in number and in the magnitude of their peak values [4]. Since yielding of the tension reinforcement across wide open cracks prevents closing of these cracks when the load is reversed, the flexural

capacity of the critical sections at high ductilities will be determined principally by the state of stress in the steel reinforcement.

This also holds true for the moment capacity of flexural members subjected to high shear if the critical regions contain sufficient shear reinforcement. This can be clearly demonstrated by using Beam 43 as an example. From monotonic tension tests, the maximum strength of the reinforcing steel was measured at 97 ksi. It seems reasonable to assume that a few stress reversals would not change this strength significantly. With only the steel participating in resisting moment, and with $p = p'$, the maximum moment capacity of the beam can be computed as

$$M_{max} = A_s f_{max} (d-d') = 6.0 \times 97 \times 21.5 = 12{,}500 \text{ kip-in.}$$

The maximum moment measured in the experiment was equal to 12,470 kip-in. Hence, in Beam 43 the compression and tension reinforcement did attain its maximum strength, and the lever arm of the internal moment was equal to the distance between the reinforcement centroids.

However, to fully describe the complete load-deformation relationship of a flexural member, it is necessary to know the moment-curvature relationship $M\text{-}\Phi$ as well as the shear force-shear deformation relationship $V\text{-}\gamma$. The two relationships are coupled, especially when the member is subjected to high shear. Under high shear the $V\text{-}\gamma$ relationship may govern the behavior of the member and may lead to failure at rather low flexural ductilities if the critical regions are not properly reinforced against shear failure. This is the case for Beam 35, which failed after the first load reversal at the low curvature ductility ratio of 3.7 (see Fig. 15). This failure cannot be attributed solely to excessive

flexural deformations, but to a combination of flexural and excessive shear deformations. Hence, in this case the useful limit of deformation, being either deflection or curvature, depends strongly on the shear resistance of the beam. It is evident from these tests that shear resistance decreases under load reversals and under the presence of large flexural deformations. For this reason the shear resistance mechanism and the effect of shear reinforcement need to be carefully studied. Such an attempt is made in the next section.

It also has to be pointed out that large shear deformations may lead to a considerable degradation in stiffness of the flexural member and consequently to a decrease in its energy dissipation capacity. This is another reason why displacement ductility alone is not a good index for describing the behavior of reinforced concrete members.

5.2 Effect of Shear

In the past, many experiments were performed on reinforced concrete beams failing in shear [9, 15-23], and the results have been evaluated statistically [24]. In almost all tests loads were increased monotonically up to failure, and consequently the mechanism of shear resistance for monotonic load application is reasonably well understood [9]. However, little is known about the effect of load reversals on the mechanism of shear resistance, and many practical design questions about the shear behavior of reinforced concrete beams subjected to load reversals remain to be answered:

1) To what extent will shear affect the rotation and the energy dissipation capacities of the beams under load reversals?

2) In what ways will load reversals affect the shear resistance mechanisms.

3) In what ℓ/d range will shear effects become important?

4) How should beams be designed to avoid shear failure under load reversals so that the required rotation and energy dissipation capacities can be attained?

The tests discussed in this report ar too small a sample to arrive at general conclusions for design criteria; however, they may serve as a basis for the further research that is urgently needed in this area.

Our experiments show that usually larger and more closely spaced stirrups significantly increase the specimens ability to resist a larger number of cycles in the inelastic range, leading to a greater energy dissipation capacity. However, when large inelastic deformations are imposed to the beam, and the beam cracks diagonally in both directions due to load reversals, the shear resistance drops significantly below that predicted by the ACI 1971 code. As an example, the predicted shear capacity of Beam 43 is equal to 258 kips, yet the beam failed in shear at a load of 160 kips, exhibiting large transverse displacements across the main diagonal cracks. The cause of this shear failure was that once the concrete core became fragmented by diagonal cracks, abrasion occured along these diagonal surfaces, and the concrete started to crumble to pieces. Therefore, a good deal of the shear had to be resisted by dowel action of the longitudinal reinforcement.

Factors causing the breakdown in shear resistance are discussed in detail below.

a) DETERIORATION OF SHEAR RESISTING CAPACITY OF STIRRUP-TIES UNDER LOAD REVERSALS. The presence of web reinforcement impedes the growth of diagonal tension cracks and reduces their penetration into the

compression zone, leaving more uncracked concrete at the head of the crack to resist the combined action of shear and compression. Closed stirrups confine the concrete core and permit larger concrete strains to be attained than in unconfined concrete. Stirrup-ties also provide support for longitudinal reinforcement so that dowel shear can develop more effectively, and buckling of the compression reinforcement is delayed.

Load reversals reduce the effectiveness of the stirrup-ties in performing these functions. After diagonal tension cracks occur, the portions of the web reinforcement where these cracks cross the stirrup-ties undergo cycles of unidirectional straining that may lead to a gradual deterioration of the bond between stirrups and concrete. Further deterioration can occur from motion of the concrete blocks along the diagonal cracks. Furthermore, if flexural and diagonal tension cracks are present in both directions from preceding load reversals, the compression zone at the tip of the diagonal tension crack may be fractured by flexural cracks. Then the shear resistance of the compression zone has to depend mainly on dowel action in the compression steel and on aggregate interlocking resistance. This, together with the deterioration in web reinforcement bond, is believed to be the main reason for the failure of beams in shear. This failure is evidenced simultaneously by a drop in resistance and large displacements across the main diagonal tension cracks.

b) DOWEL ACTION AND LOSS OF BOND IN LONGITUDINAL STEEL BARS: Bond stresses in the longitudinal bars tend to build up close to the flexural cracks and can lead to a deterioration of bond under cyclic loading [4]. The prying action of the dowel shear accelerates the

deterioration of bond between the longitudinal steel and the concrete. As a consequence, the composite action of steel and concrete deteriorates and the beam stiffness decreases. Prying action may cause splitting along the deformed steel bars, as can be seen in Fig. 20.

c) ABRASION OF CRACKED SURFACES AND AGGREGATE INTERLOCKING RESISTANCE: The nature of aggregate interlocking shear resistance under monotonic loading was investigated by Fenwick and Paulay [20] who formulated a semiempirical equation for its analysis. Aggregate interlocking shear is related to the width of the diagonal tension cracks, shear displacements across the cracks and concrete strength. This kind of resistance is weakened under load reversals by abrasion of the two contacting surfaces at the cracks. Surface granules wear off, crack width may increase, and interlocking resistance may deteriorate substantially.

A combination of these effects can lead to a shear failure under smaller loads than predicted by the ACI 1971 Code. Fig. 21 illustrates a tentative shear failure mechanism that includes all these deteriorating effects.

An estimate of the contribution of shear deformations to the tip deflection of the three test specimens is illustrated in Fig. 22. Tip deflection is separated into three components in these graphs. The δ^1_{flex} component is tip deflection caused by fixed end rotation and beam rotation within 17.25 in. from the fixed end of the centilever. This component was computed as

$$\delta^1_{flex} = (6\bar{\Phi}_1)75 + (11.25\Phi_2)66.375$$

where $\bar{\Phi}_1$ and Φ_2 are taken from Figs. 15-17. The δ^2_{flex} component is an estimate of deflection due to flexural deformation within the remaining 60.75 in. of the cantilever. Since the moment in this range was smaller than the yield moment, δ^2_{flex} was computed from the elastic properties of the cracked section that can be estimated from

$$(EI)_{cr} = \frac{78^3 \times K_2}{3}$$

where K_2 is the measured cracked elastic stiffness obtained from the load-deflection diagrams in Figs. 11-14. The remaining deflection, δ_{shear} shown cross hatched in Fig. 22, can then be considered an estimate of the deflection caused by shear deformations along the beam.

Tip deflection due to shear deformations based on the elastic properties of the concrete ($\gamma = \tau/G$ with $\tau = V/bd$) amounts to only 0.017 in. at the failure load of Beam 35. Hence, it can be seen that most of the tip deflection due to shear deformations is caused by transverse displacements across the diagonal tension cracks. These cracks are concentrated in the critical region of the beam and extend about 34 in. for Beam 35, 30 in. for Beam 46, and 23 in. for Beam 43 from the root of the cantilever.

Figure 22 clearly shows the superior behavior in shear of Beam 43 compared to Beams 35 and 46, especially since Beam 43 resisted deflections far beyond the last point (65) indicated in Fig. 22.

SHEAR CAPACITY OF THE BEAMS: The shear capacities of the three test specimens as computed from the ACI Code ($V_{ult} = V_c + V_s$) are listed in Table 2. The equations given in the ACI Code are based on monotonic loading and on the assumption that concrete participates

in resisting shear even after diagonal tension cracking has occurred. The computed shear capacities differ significantly from specimen to specimen because of the variation in the size and spacing of the stirrup-ties; for example, the shear capacity of Beam 43 is 2.3 times larger than that of Beam 35.

Beam 35 exceeded the computed capacity by 9 percent despite cyclic loading but failed after the first load reversal at a deflection ductility ratio of $\mu = 3.3$ (see Fig. 12). Figure 22 shows large shear deformations at this level. Beam 46 did not reach the computed shear capacity due to the brittle fracture of a reinforcing bar, but shear deformations at failure were significantly smaller than in Beam 35. The maximum shear that Beam 43 resisted was only 62 percent of that predicted by the ACI Code (160 kips vs. 258 kip). However, the specimen resisted a large number of load reversals and attained its maximum moment capacity at a deflection ductility ratio of $\mu = 6.25$ i.e., at a tip deflection of 3.33 in. At this level of deflection the shear resistance of the beam had already been significantly reduced by the crumbling of the concrete core.

The tests showed that an increase in the number and size of stirrup-ties proved to be beneficial for the following reasons:

1) Shear deformations in the beams after diagonal tension cracking has occurred are reduced. This increases the stiffness of the beam and leads to hysteresis loops with large enclosed areas.

2) Deterioration in beam stiffness for the second cycle of the same deflection amplitude is reduced.

3) The number of cycles beams can sustain before failure is increased.

4) Shear failure occurrs at larger average curvatures, and the rotation capacity of the inelastic regions in the beams increases significantly.

However, at large inelastic deformations and cyclic loading, shear failure could not be prevented by additional web reinforcement in the shear span-depth ratio investigated ($\ell/d = 3.1$). In fact, for Beam 43, the shear capacity of the section was smaller than V_s, the yield capacity of the stirrup ties alone. Hence the truss analogy usually taken as the basis for designing web reinforcement cannot be applied if the concrete core is severely damaged from load reversals. It is also important to note that Beam 43 failed in shear at a nominal shear stress of

$$v_{max} = \frac{V_{max}}{bd} = 422 \text{ psi} \cong 6\sqrt{f'_c}$$

This value is substantially below $10\sqrt{f'_c}$ given in the ACI 1971 Code as the lowest limiting value for use in the shear design equations of Section 11.6. (The code recommends $(v_u - v_c) \leq 8\sqrt{f'_c}$ with v_c of at least $2\sqrt{f'_c}$). It should be emphasized that the equations recommended in the ACI Code were derived from results obtained in tests carried out under monotonically increasing loading. In view of the results reported in this investigations and by other investigators [8,25], applying these equations to seismic design as recommended in Appendix A of the ACI 1971 Code is questionable.

5.3 Stiffness Deterioration

Stiffness deterioration in reinforced concrete members subjected to load reversals has been studied experimentally by several

investigators [4,8,26,27,28], and various analytical stiffness-degrading hysteresis models have been proposed in the literature [21,30,31]. However, none of these models include the effect of shear deformations on the stiffness degradation of flexural members.

An estimate of the effect of shear forces on the stiffness degradation of the test specimen can be obtained from a study of the load-tip deflection relationship, since deflection caused by shear deformations is included in this relationship.

Stiffness degradation, exemplified by the P-δ graphs, is illustrated in Figs. 23-25. In these figures some of the loading and unloading curves for the three specimens (shown earlier in Figs. 12-14) are shifted to the same origin, allowing a comparison of stiffnesses for different values of tip deflections. The following observations can be made from these graphs.

1) Stiffness deterioration is directly related to the magnitude of the tip deflection and to the extent of cracking in the critical regions.

2) After significant cracking takes place in the critical regions of the beam, the loading stiffness varies according to the following main characteristics: The initial loading stiffness is small since at this stage the cracks are open and only the steel participates in resisting moments; when the cracks close, the stiffness of the beam increases and then drops off again when the longitudinal reinforcement starts to yield.

3) Shear deformations cause a further decrease in the initial loading stiffness and lead to a pronounced pinched shape of the P-δ hysteresis loops. This pinching increases when the peak values of the deformations increase.

4) Deterioration of the loading stiffness is significantly larger than deterioration in the unloading stiffness. However, the latter effect should also be included in a refined stiffness-degrading model, since the unloading stiffness in Beam 43, for example, at a deflection ductility ratio of four is only about one-half of the unloading stiffness at first yielding (points 33 and 65 in Fig. 25).

Deterioration in stiffness before first yieldings of the main reinforcement occurs can be estimated from Fig. 11.

Deterioration in stiffness from the first to the second cycle of the same deflection amplitude is illustrated in Fig. 26. As can be seen from the graphs, the unloading stiffness remains essentially unchanged. The difference between the first loading curve and the first reloading curve is marked in the graphs by horizontal lines. As can be seen, the first reloading to the previously attained displacement level shows a rather significant deterioration in stiffness. This deterioration is caused by a combination of increasing permanent flexural and shear deformation. The difference between the first and second reloading curve is marked by vertical lines. Here the deterioration in stiffness is smaller and is caused mainly by an increase in shear deformations, since the corresponding stiffnesses of the M-Φ diagrams in Figs. 15-17 remain essentially the same. It is believed that with proper shear reinforcement and proper confinement of the concrete core, deterioration in stiffness after the first reloading can be minimized and stable, repeatable hysteresis loops can be achieved. This can be seen in Fig. 26 by comparing the small deterioration in the loops of Beam 43 to the significant deterioration present in the loops of Beam 35.

5.4 Ductility and Rotation Capacity

In the literature, the ductility factor (the ratio of maximum deformation to deformation at first yielding) has been used to measure the performance of structural components that have to sustain inelastic deformations prior to failure. Such ductility factors can be applied to strain, curvature, rotation, and displacement. Since displacement ductility factors are strongly dependent on the length of the beam and on loading conditions, and rotation ductility factors depend on the length of the critical regions, they should only be used for comparing geometrically similar beams but not as basic parameters describing the performance of the structural element. The basic parameter should be the one independent of the length of the element, which is the average curvature ductility factor.

The difficulty in characterizing the performance of the beams tested lies in the fact that the useful limit of curvature is not determined by the moment associated with the curvature but by shear forces. Furthermore, the total beam deflection at high inelastic deformations cannot be obtained by integrating the curvatures twice, since shear deformations contribute significantly to tip deflections (see Fig. 22).

The curvature ductility factors for the three specimens can be obtained from Figs. 15-17. The maximum curvature ductility factor for Beam 35 is equal to 4, that for Beam 43 is equal to 11. Hence it is evident that increasing the amount of web reinforcement can significantly increase the curvature ductility.

A clear picture of the superior behavior of Beam 43 can be obtained from Table 4 in which the maximum ductility factors for Beam 35 and Beam 43 are listed. Beam 46 is omitted, because its failure was

caused by a brittle fracture of one of the reinforcement bars. This table also shows the maximum plastic rotations θ_{pl} in the critical regions of the two specimens. These critical regions were assumed to extend from the fixed end of the cantilever to the last point of curvature measurement, which was at a distance of 17.25 in. from the fixed end. The rotation θ_{pl} can then be obtained from Fig. 22 as

$$\theta_{pl} = \frac{\Delta \delta^{1}_{flex}}{78 - \frac{17.25}{2}}$$

where $\Delta \delta^{1}_{flex}$ is equal to the difference between δ^{1}_{flex} at maximum deflection and δ^{1}_{flex} at yield deflection.

Beam 35 developed a maximum plastic rotation of 0.016 rad; the authors believe that this rotation capacity is inadequate for critical regions in flexural members. This inadequacy is even more apparent when it is observed that an appreciable portion of this rotation may be caused by the previously discussed fixed end rotation, θ_{FE}, and not by flexural deformations within the beam. It should also be noted that the deflection ductility factor corresponding to flexural deformations alone (with deflections due to shear deformations subtracted) reaches only a value of 2.6.

The last column in Table 4 contains the cumulative rotations obtained by summing up the rotations after first yielding from zero load to the points of load reversals for all cycles up to failure. This can be considered a measure of the flexural deformational capacity of the member.

Since all tested beams were doubly reinforced with p = p', the ductility of the beams may have been improved by the presence of the large amount of compression steel [1]. Moreover, since both tension and compression reinforcement was placed in two layers, the dowel resistance was probably increased, which contributed indirectly to the ductility by delaying beam failure in shear. Hence, the ductilities obtained are higher than what may be expected when reinforcement is placed in single layers and for p' smaller than p.

Reference 4 shows that load reversals lead to an increase in ductility if a beam is subjected to pure bending (very large ℓ/d). However, under the presence of large shear forces (small ℓ/d and large percentages of steel p and p'), severe load reversals may lead to a premature deterioration of the shear resistance mechanism of the critical flexural regions. Because of the detrimental effect of this deterioration on the energy dissipation characteristics of reinforced concrete beams, the importance of proper shear reinforcement in ductile moment-resistant frames subjected to load reversals has to be emphasized.

5.5 Energy Absorption and Energy Dissipation

Since energy in the specimens is absorbed by flexural and shear deformations, the following discussion is based on a study of the P-δ hysteresis loops rather than on a study of the M-Φ hysteresis diagrams.

Figure 26 shows several hysteresis loops for the three specimems tested. It is clear that a stiffness degrading model is required to represent these hysteresis loops realistically. If we consider only cycles after first yielding, the model proposed by Clough [31] with a modification for the unloading stiffness seems to be sufficiently

accurate to represent all hysteresis loops, provided that excessive shear deformations and consequent pronounced pinching of the hysteresis loops are prevented by proper shear reinforcement.

The basis for Clough's model is a bilinear diagram consisting of an elastic stiffness (based on the properties of the cracked section), and a strain-hardening stiffness. The reloading stiffness after yielding in the direction of the loading is then always determined by connecting the point of zero load with the point of maximum deformation that has occurred at any previous time. This point is obviously located on the bilinear virgin curve. The reloading stiffness before yielding in the direction of loading is obtained by connecting the point of zero load with the yield point of the virgin curve. The modification suggested for this model consists of varying the unloading stiffness K corresponding to the ductility factor μ at which unloading takes place. This is done so as to account for the stiffness deterioration on unloading. Such a modification could take the following form

$$K = K_e \left(\frac{1}{\mu}\right)^{\alpha}$$

where K_e is the elastic stiffness and α is an experimentally determined exponent, whose determination is beyond the scope of this investigation.

The model discussed is illustrated for two loops of Beam 43 in Fig. 27. In the authors' opinion, the agreement achieved with this model is sufficiently accurate for a realistic earthquake analysis of structures, provided that excessive shear deformations are prevented. The main problem arising in the analysis is not to model the hysteretic behavior exactly point by point but to model reasonably well the general shape of the hysteresis loop and to determine a safe limit for applying the model.

The proposed model accounts for most of the decrease in energy dissipated from the first to the second cycle of the same deformation amplitude; however, no further deterioration is exhibited if more than two cycles of the same amplitude are carried out. If sufficient shear reinforcement is provided and the amplitude of the cycles remains well below the useful limit of deformation, it is believed that the loops stabilize for several cycles after the second cycle and that the proposed model is sufficiently accurate. If the amplitude approaches the useful limit of deformation which depends on the loading history, or if shear reinforcement is inadequate, the model would have to include further stiffness and strength degrading properties.

The proposed model cannot be applied before first yielding of the main reinforcement occurs, since only one average elastic stiffness is assumed. For the pre-yielding range, the more refined trilinear model proposed by Takeda et al. [32], which has an uncracked and a cracked "elastic" stiffness, can be applied. This model accounts for the energy dissipation caused by cracking of the concrete.

6. SUMMARY

This report presents and discusses the results obtained in a preliminary investigation of the behavior of flexural R.C. regions subjected to severe reversals of bending moments and high shear forces. The experimental studies were carried out on three large size cantilever beams. All three beams had the same longitudinal reinforcement but different shear reinforcement.

The main objective of the investigation was to study the effects of the high shear forces on the deformation, strength, stiffness

and energy dissipation capacity of the beams. At the present state of the study no general conclusions can be formulated, since only three specimens have been tested and a large number of important parameters could not be investigated. However, from the evaluation of the available test results the following main observations can be made.

1) The behavior of flexural members after one or more severe reversals of high shear forces is quite different from that observed in a monotonically increasing loading test.

2) When the concrete core of the critical regions is properly confined and adequate reinforcement against the effect of high shear is provided, these regions can attain high moment capacities as well as large curvature and rotation ductilities.

3) To fully describe the behavior of a flexural member it is necessary to know the moment-curvature relationship M-Φ as well as the shear force - shear deformation relationship V-γ. The two relationships are coupled at the critical regions.

4) Slippage of the reinforcement in the anchorage zone may decrease significantly the stiffness of the member

5) Under high shear the V-γ relationship may govern the behavior of the member which may lead to failures at rather low flexural ductilities if the critical regions have inadequate web reinforcement.

6) The shear resistance of a flexural member is reduced once large reversals of flexural deformations (beyond yielding) are induced.

7) The deterioration in the shear resistance under load reversals can be attributed to the following causes: a) reduction in the effective compression zone due to flexural cracking in previous load cycles; b) deterioration of the interlocking resistance due to abraded concrete surfaces; c) deterioration of bond along stirrup-ties; d) loss of bond in main reinforcement and splitting of concrete cover.

8) When the "truss action", i.e. the composite action of concrete and stirrup-ties deteriorates, shear is carried mainly by dowel action of the main reinforcement.

9) Most of the shear-type deformations are caused by large transverse displacements across one or two pairs of intersecting main diagonal tension cracks.

10) The shear resistance increases with closer spacing and larger sizes of stirrup-ties, however it does not increase linearly with the amount of web reinforcement.

11) When critical flexural regions are subjected to load reversals, the application of the design equations for shear reinforcement recommended by the ACI 1971 Code (Section 11.6) is questionable. From experimental evidence it appears to be advisable to neglect the shear resistance of the concrete, V_c, in the shear design of flexural members subjected to load reversals.

12) If the shear deformations in a flexural member are small, the P-δ hysteresis loops are of "spindle shape". Large shear-type deformations lead to a pronounced "pinching" of the hystesesis loops and consequently to a decrease in the energy dissipation capacity.

13) The deterioration in stiffness of the flexural members is a function of the maximum flexural and shear deformations experienced by the member.

14) The deterioration in stiffness after first reloading in successive cycles of the same displacement amplitude is caused mainly by additional shear deformations.

15) If large shear deformations do not occur, the hysteresis model proposed by Clough [31] closely simulates the experimental hysteresis loops.

16) Further research should be directed towards determining a "useful deformation limit" for hysteresis models. Beyond such a limit no reliance can be placed upon the properties of the model. This limit is a function of the loading history as well as the maximum flexural and shear deformations developed at the critical regions. Consequently a realistic V-γ relationship has to be incorporated into the hysteresis model and special attention has to be paid to the amount and detailing of web reinforcement.

REFERENCES

1. Blume, J. A., Newmark, N. M., and Corning, L. H., "Design of Multistory Reinforced Concrete Buildings for Earthquake Motions," Portland Cement Association, Chicago, 1961.

2. "Building Code Requirements for Reinforced Concrete (ACI 318-71)" American Concrete Institute, 1971.

3. ACI Committee 439, "Effect of Steel Strength and of Reinforcement Ratio on the Mode of Failure and Strain Energy Capacity of Reinforced Concrete Beams," ACI Journal, Proceedings, Vol. 66, No. 3, March 1969.

4. Bertero, V. V., Bresler, B., and Liao, H., "Stiffness Degradation of Reinforced Concrete Members Subjected to Cyclic Flexural Moments," Report No. EERC 69-12, Earthquake Engineering Research Center, College of Engineering, University of California, Berkeley, December 1969.

5. Park, R., Kent, D., and Sampson, R., "Reinforced Concrete Members with Cyclic Loading," Journal of the Structural Division, ASCE, Vol. 98, No. ST7, July 1972.

6. Umemura, H., and Aoyama, H., "Evaluation of Inelastic Seismic Deflection of Reinforced Concrete Frames Based on the Tests of Members," Proceedings of the Fourth World Conference on Earthquake Engineering, Chile, 1969, Volume I.

7. Ruiz, M., and Winter, G., "Reinforced Concrete Beams Under Repeated Loads," Journal of the Structural Division, ASCE, Vol. 95, No ST6, June 1969.

8. Brown, R. H., and Jirsa, J. O., "Reinforced Concrete Beams Under Load Reversals," ACI Journal, Proceedings, Vol. 68, No. 5, May 1971.

9. Bresler, B., and MacGregor, J. G., "Review of Concrete Beams Failing in Shear," Journal of the Structural Division, ASCE, Vol. 93, No. ST1, February 1967.

10. "Building Code Requirements for Reinforced Concrete (ACI 318-63)," American Concrete Institute, June 1963.

11. Bouwkamp, J. G., and Stephen, R. M., "Cyclic Loading of Full-Size Tubular Joints," Service to Industry Report No. 70-1, Department of Civil Engineering, University of California, Berkeley, February 1970.

12. Popov, E. P., and Stephen, R. M., "Cyclic Loading of Full-Size Steel Connections," Report No. EERC 70-3, Earthquake Engineering Research Center, College of Engineering, University of California, Berkeley, July 1970.

13. Bertero, V. V., and Felippa, C., Discussion of "Ductility of Concrete," by Roy, H.E.H., and Sozen, M. A., Proceedings of the International Symposium on Flexural Mechanics of Reinforced Concrete, ASCE - ACI, Miami, November 1964.

14. Agrawal, G. L., Tulin, L. G., and Gerstle, K. H., "Response of Doubly Reinforced Concrete Beams to Cyclic Loading," ACI Journal, Proceedings, Vol. 62, No. 7, July 1965.

15. Bernaert, S., and Siess, C. P., "Strength in Shear of Reinforced Concrete Beams under Uniform Load," Civil Engineering Studies, Structural Research Series No. 120, University of Illinois, June 1956.

16. Taylor, R., "Some Shear Tests on Reinforced Concrete Beams without Shear Reinforcement," Magazine of Concrete Research, Vol. 12, No. 36, November 1960.

17. Krefeld, W. J., and Thurston, C. W., "Contribution of Longitudinal Steel to Shear Resistance of Reinforced Concrete Beams," ACI Journal, Proceedings, Vol. 63, No. 3, March 1966.

18. Krefeld, W. J., and Thurston, C. W., "Studies of the Shear and Diagonal Tension Strength of Simply Supported Reinforced Concrete Beams," ACI Journal, Proceedings, Vol. 63, No. 4, April 1966.

19. Zielinski, Z. A., "Behavior and Ultimate Strength of Rectangular Reinforced Concrete Beams in Bending and High Shear," Bulletin No. 81, Engineering School Bulletin, North Carolina State University, September 1967.

20. Fenwick, R. C., and Pauley, T., "Mechanism of Shear Resistance of Concrete Beams," Journal of the Structural Division, ASCE, Vol. 94, No. ST10, October 1968.

21. Broms, B. B., "Shear Strength of Reinforced Concrete Beams," Journal of the Structural Division, ASCE, Vol. 95, No. ST6, June 1969.

22. Placas, A., and Regan, P. E., "Shear Failure of Reinforced Concrete Beams," ACI Journal, Proceedings, Vol. 68, No. 10, October 1971.

23. Haddadin, M. J., Hong, S., and Mattock, A. H., "Stirrup Effectiveness in Reinforced Concrete Beams with Axial Forces," Journal of the Structural Division, ASCE, Vol. 97, No. ST9, September 1971.

24. Zsutty, T., "Shear Strength Prediction for Separate Categories of Simple Beam Tests," ACI Journal, Proceedings, Vol. 68, No. 2, February 1971.

25. Kano, Y., et al., "Shear Strength of Reinforced Concrete Beams Under Many Cyclic Alternate Loading," Research Report of A.I.J. August 1969.

26. Arakawa, T., et al., "Shear Strength of Reinforced Concrete Members Subjected to Alternately Cyclic Loading," Research Report of A.I.J., 1970.

27. Umemura , H., Aoyama, H., and Itao, M., "Experimental Studies on Reinforced Concrete Members and Composite Steel and Reinforced Concrete Members," Laboratory Report, University of Tokyo, December 1970.

28. Bertero, V. V., McClure, G., and Popov, E. P., "Behavior of Reinforced Concrete Frames Subjected to Repeated Reversible Loads," Report Series 100, Issue 18, Structures and Material Research, Department of Civil Engineering,University of California, Berkeley, January 1962.

29. Hanson, N. W., "Seismic Resistance of Reinforced Concrete Beam-Column Joints," Journal of the Structural Division, ASCE, Vol. 93., No. ST5, October 1967.

30. Paulay, T., "Simulated Seismic Loading of Spandrel Beams," Journal of the Structural Division, ASCE, Vol. 97, No. ST9, September 1971.

31. Clough, R. W., "Effect of Stiffness Degradation on Earthquake Ductility Requirements," Report No. 66-16, Structures and Materials Research, Department of Civil Engineering, University of California, Berkeley, October 1966.

32. Takeda, T., Sozen, M. A., and Nielsen, N. N., "Reinforced Concrete Response to Simulated Earthquakes," Journal of the Structural Division, ASCE, Vol. 96, No. ST12, December 1970.

33. Gulkan, P., and Sozen, M. A., "Response and Energy Dissipation of Reinforced Concrete Frames Subjected to Strong Base Motions," Civil Engineering Studies, Structural Research Series No. 377, University of Illinois, May 1971.

TABLE 1. SPECIMEN PROPERTIES

PARAMETERS	BEAM 35*	BEAM 46	BEAM 43
ℓ (in)	78.0	78.0	78.0
h (in)	29.0	29.0	29.0
b (in)	15.0	15.0	19.0
d (in)	25.25	25.25	25.25
d'(in)	3.75	3.75	3.75
$A_s(in^2)$	6.00	6.00	6.00
$A'_s(in^2)$	6.00	6.00	6.00
p	0.0158	0.0158	0.0158
p'	0.0158	0.0158	0.0158
p_b (compression reinforcement is neglected)	0.0235	0.0242	0.0336
f_y for main reinf. (ksi)	67.0	67.0	60.0
f_{max} for main reinf. (ksi)	103.0	103.0	97.0
f_y for stirrup-ties (ksi)	53.0	60.0	60.0
f_{max} for stirrup-ties (ksi)	90.0	96.0	96.0
f'_c (ksi)	3.86	3.99	5.03
design criteria	ACI- 63 Code	ACI- 63 Code, except V_u taken by stirrups only	ACI- 71 Code, Reference 1, V_u taken by stirrups only
stirrup-ties size	# 3	# 4	# 4
stirrup-ties spacing (in)	4.5*	6.0	3.0

* The stirrup-tie spacing used was 4.5 in., but for simplicity the specimen was called Beam 35 and not Beam 34.5.

TABLE 2. COMPUTED STRENGTH OF SPECIMENS

Computed Values of	Beam 35	Beam 46	Beam 43
M_{cr} (kip-in)	1510	1690	1680
M_{wl} (kip-in)	2960	3040	3160
M_c (kip-in)	3860	3940	4370
M_u (ACI-63) (kip-in)	8600	8530	8040
M_u (Ref. 1) (kip-in)	13300	13300	12500
V_{cr} (kip)	19.4	21.7	21.6
V_{wl} (kip)	38.0	39.0	40.5
V_c (kip)	49.5	50.5	56.0
V_u (ACI-63) (kip)	110.1	109.3	103.1
V_u (Ref. 1) (kip)	170.5	170.5	160.5
V_s (kip)	65.3	101.0	202.0
$V_{ult}=V_c+V_s$ (kip)	114.8	151.5	258.0

TABLE 3. PRINCIPAL EXPERIMENTAL RESULTS

Measured Values of	Beam 35	Beam 46	Beam 43
M_{cr} (kip-in)	1700	1800	1800
M_c (kip-in)	4290	4680	5070
M_y (kip-in)	9130	9130	9360
M_{max} (kip-in)	9750	10700	12470
V_{cr} (kip)	22	23	23
V_c (kip)	55	60	65
V_y (kip)	117	117	120
V_{max} (kip)	125	137	160
δ_y (in)	0.76	0.75	0.60
δ_{max} (in)	2.52	2.50	3.75
δ_{max}/ℓ	0.032	0.032	0.048
$\mu_{max}=\delta_{max}/\delta_y$	3.32	3.33	6.25

TABLE 4. DUCTILITY AND ROTATION CAPACITY

Specimen	Curvature Ductility Factor*	Flexural Deflection Ductility Factor	Total Deflection Ductility Factor	Maximum Plastic Rotation** θ_{pl} (rad)	Cumulative Rotation** $\Sigma\ \theta$ (rad)
Beam 35	3.7	2.6	3.3	0.016	0.125
Beam 43	11.0	5.4	6.25	0.034	0.607

* These average curvature ductility factors were obtained from measurements that include the fixed end rotation θ_{FE}.

** Taken over a length of 17.25 in. $\simeq$ 0.7d at the root of the cantilever.

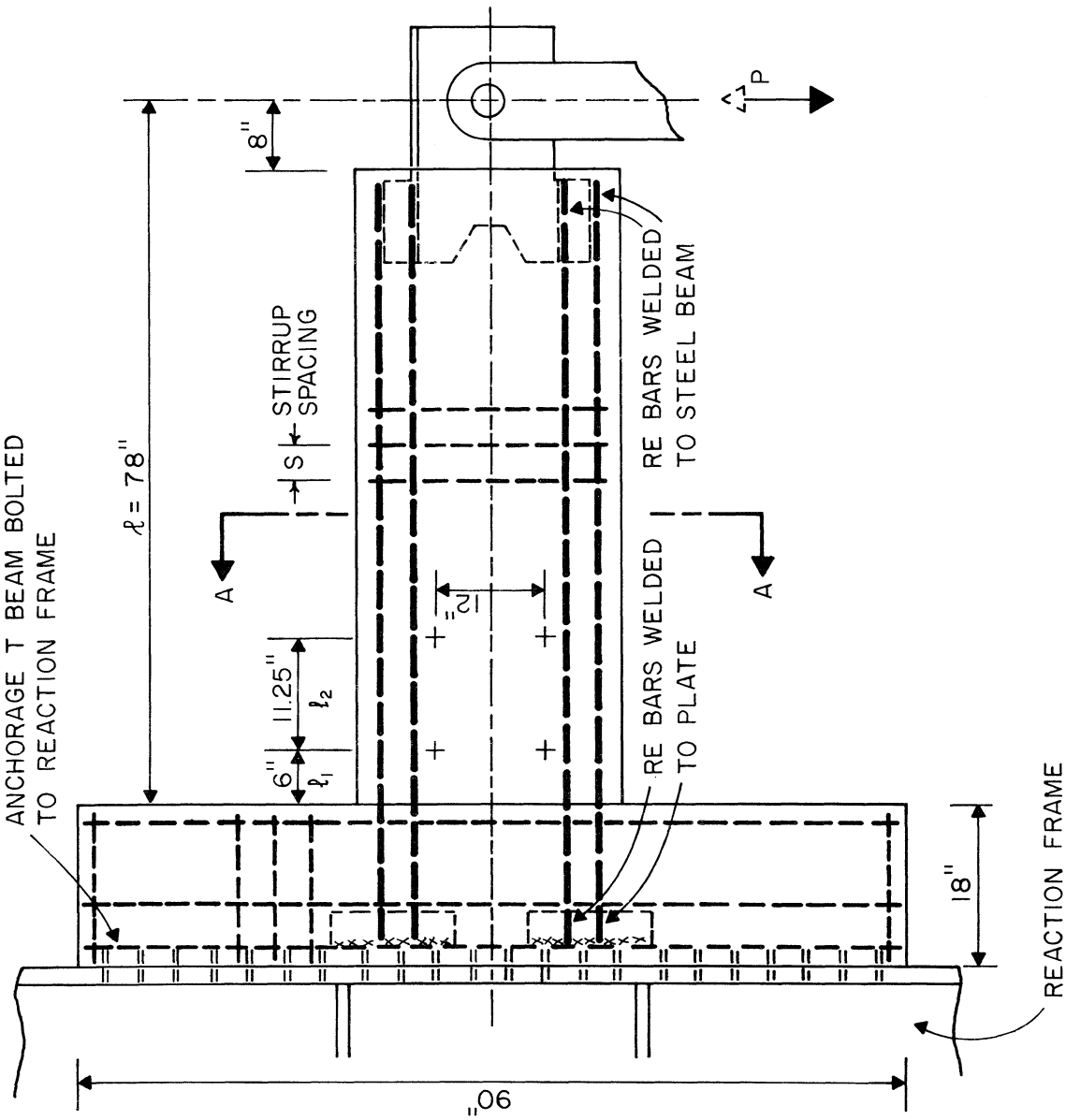

FIG. 1 TYPICAL TEST SPECIMEN

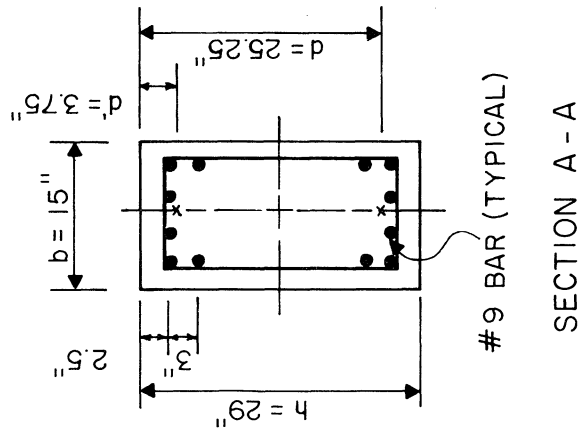

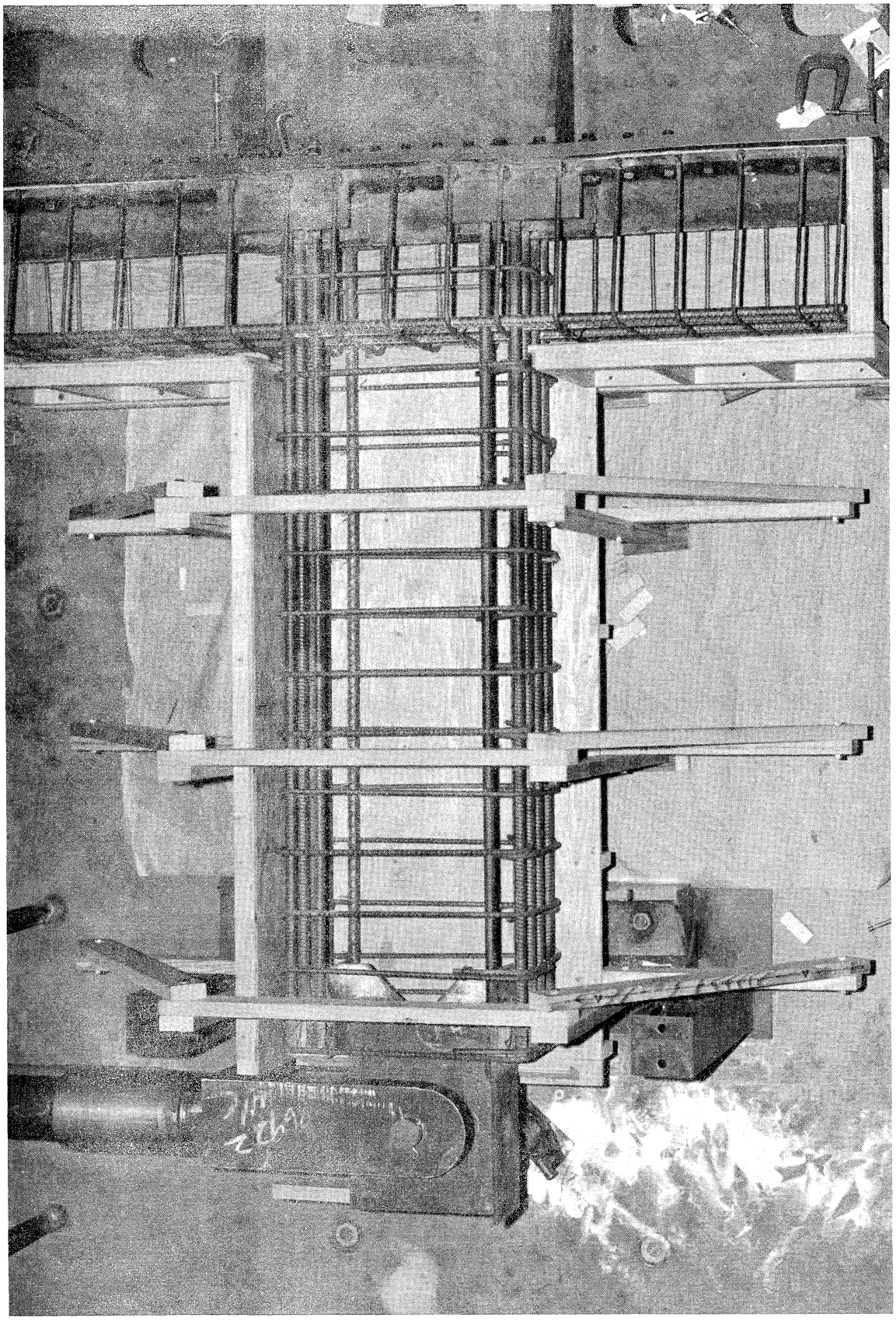

FIG. 2 REINFORCEMENT FOR BEAM 46

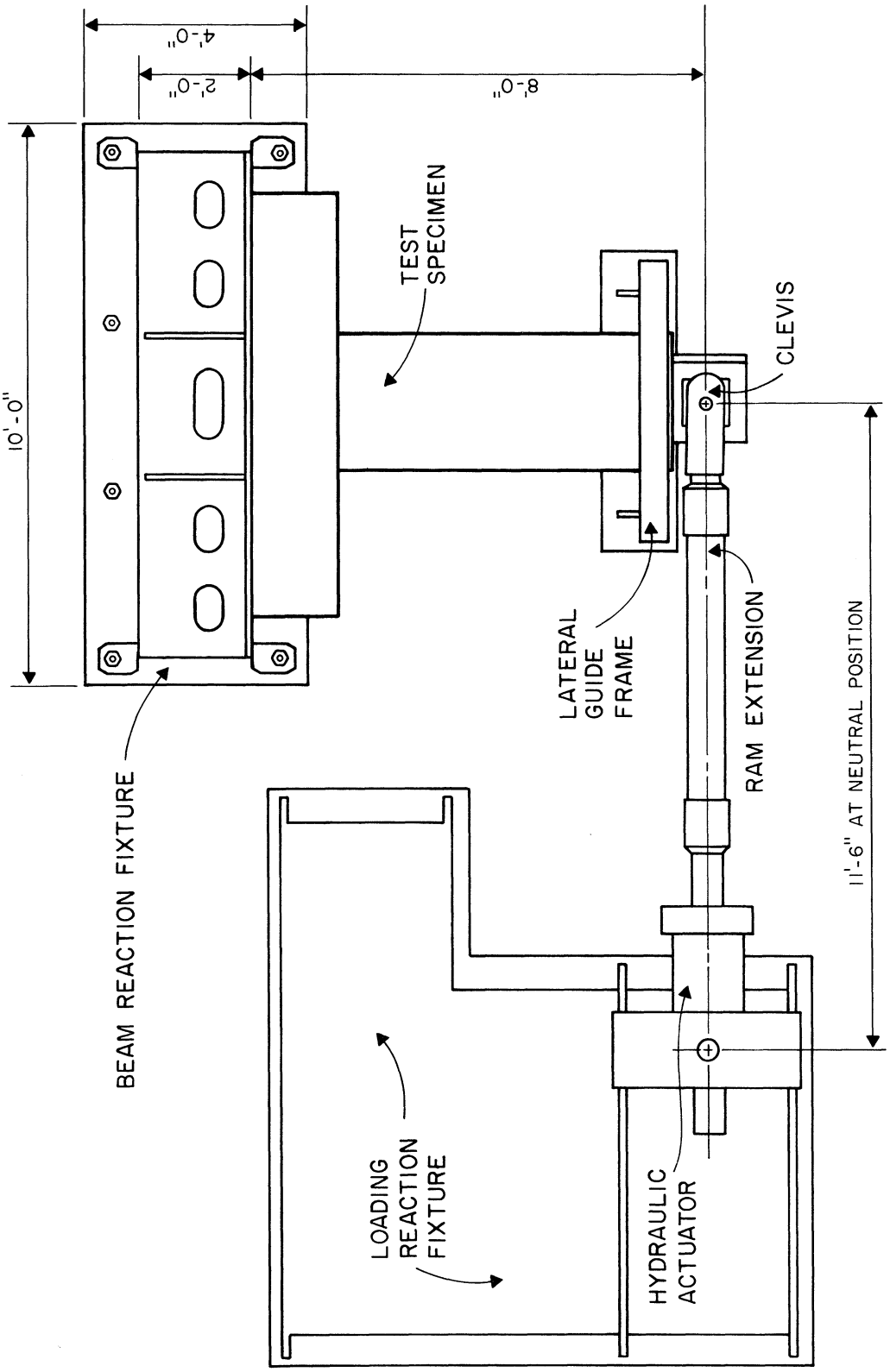

FIG. 3 SPECIMEN IN TEST FIXTURE

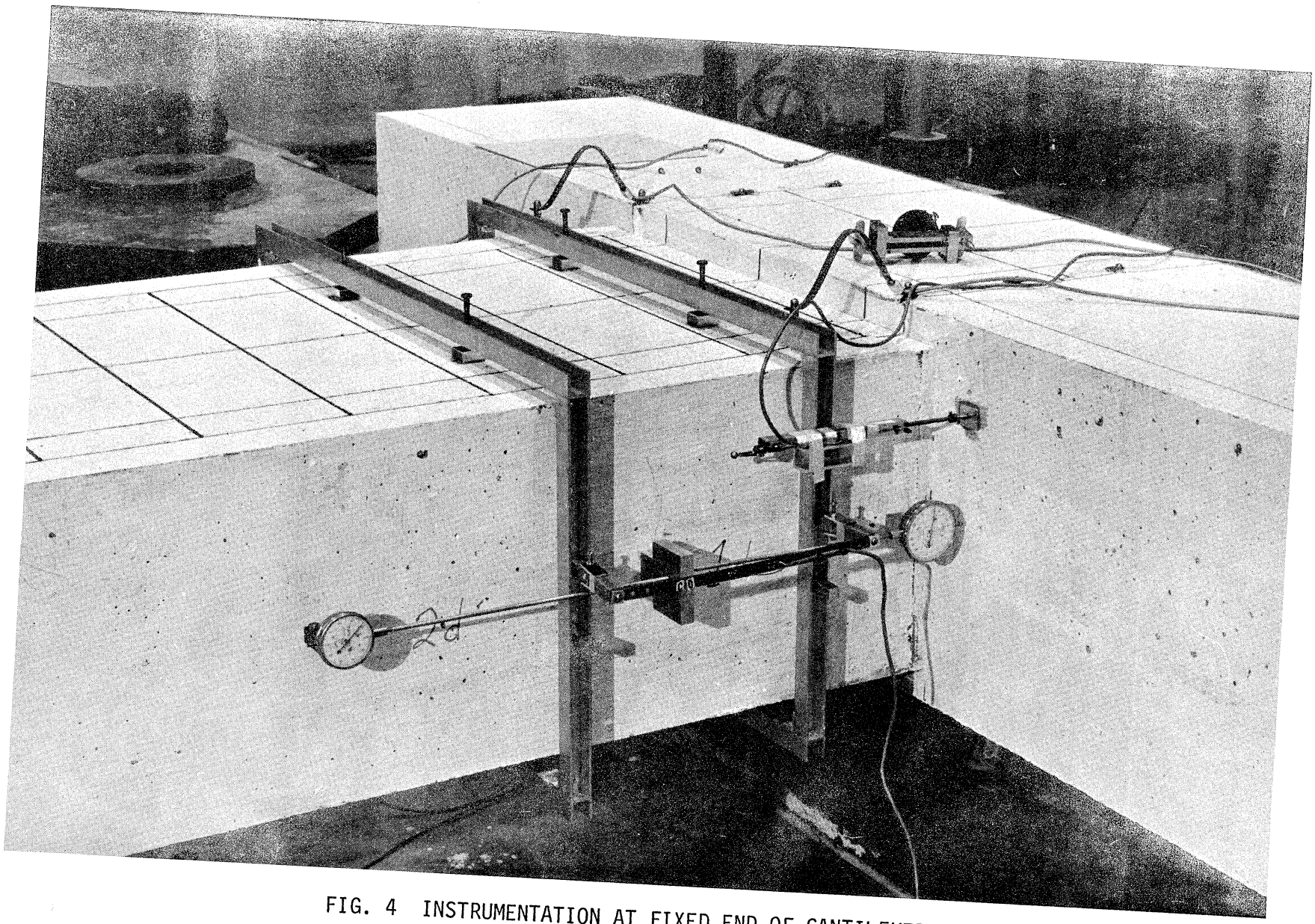

FIG. 4 INSTRUMENTATION AT FIXED END OF CANTILEVER

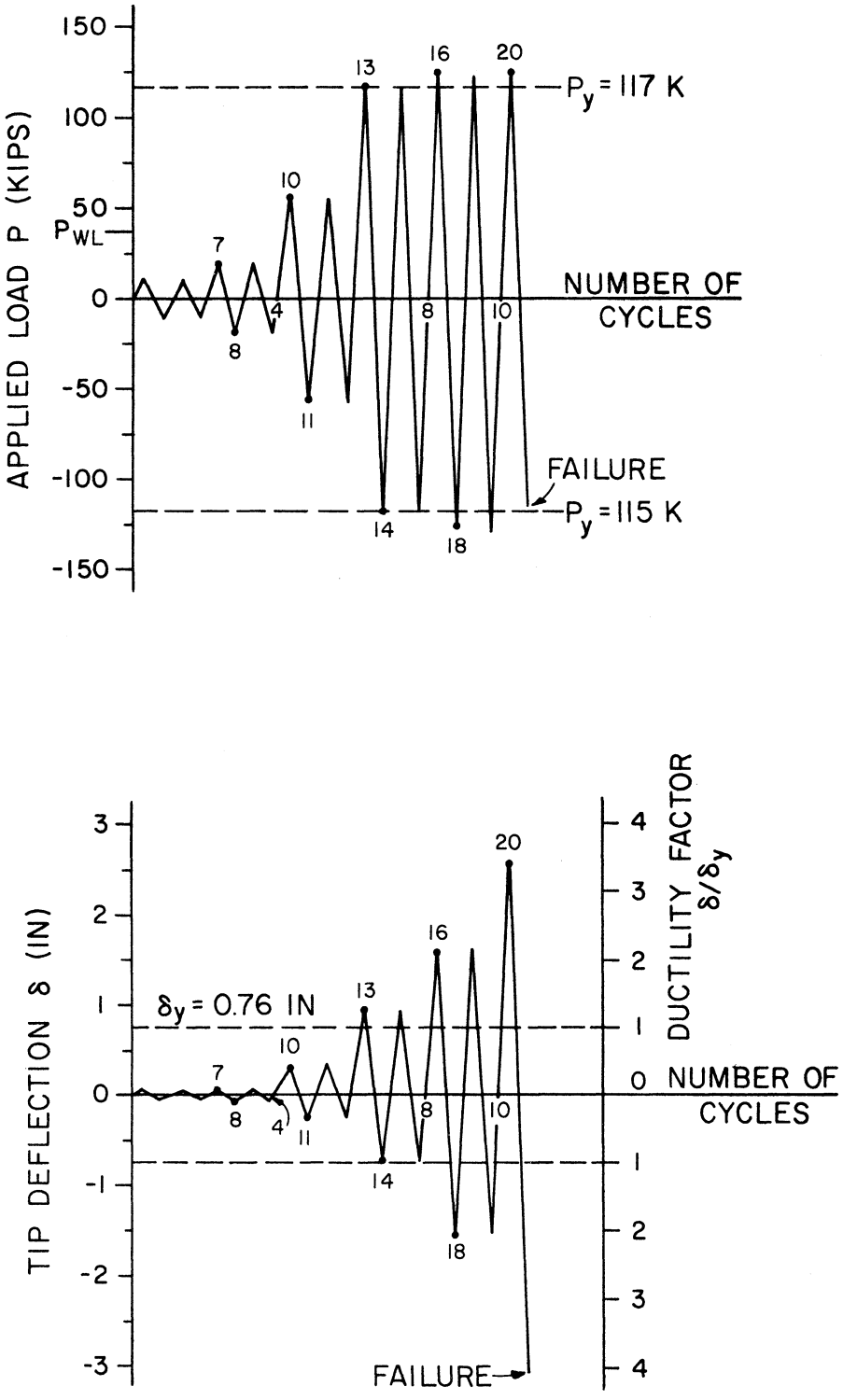

BEAM 35

FIG. 5 LOADING PROGRAM -- BEAM 35

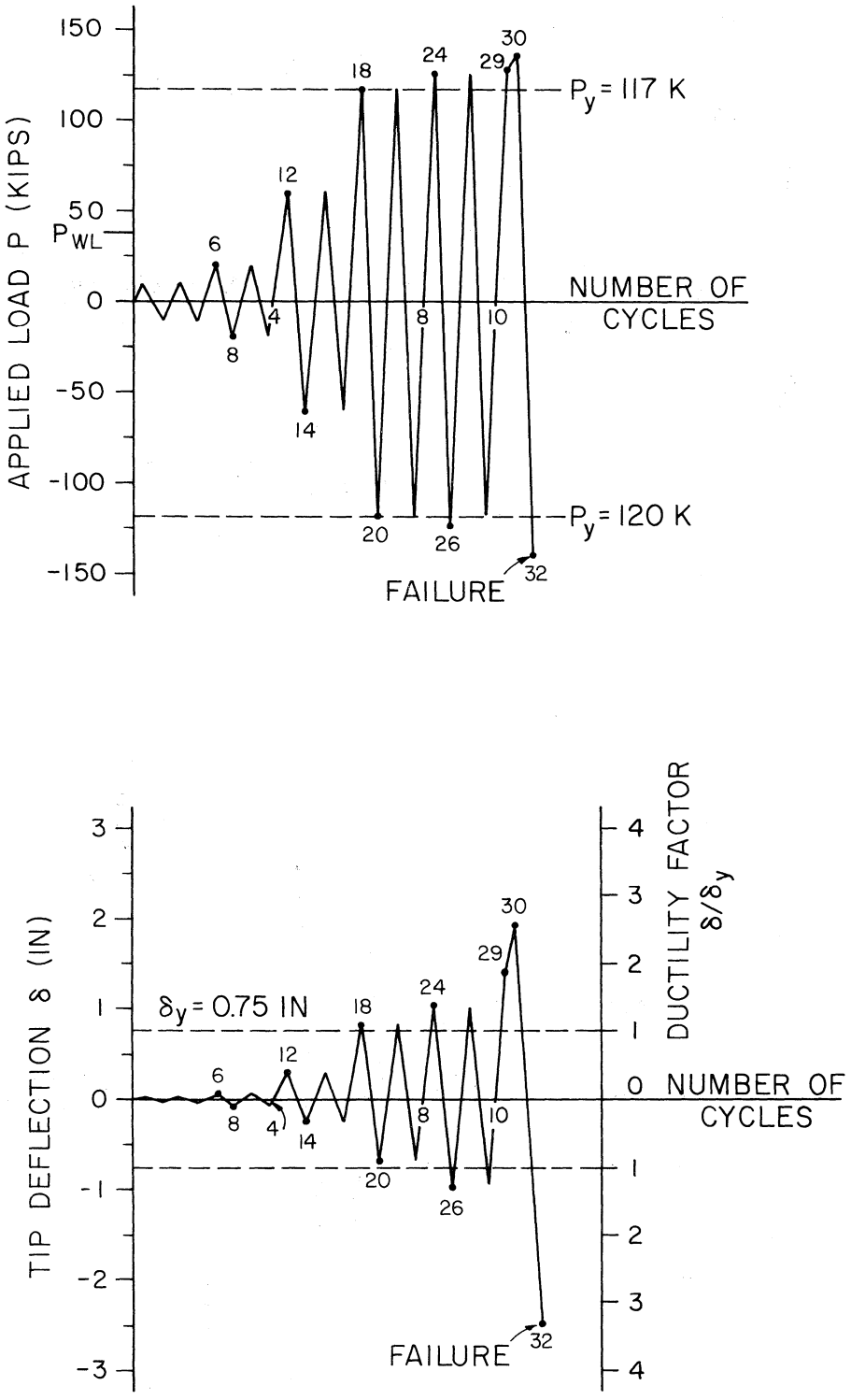

FIG. 6 LOADING PROGRAM -- BEAM 46

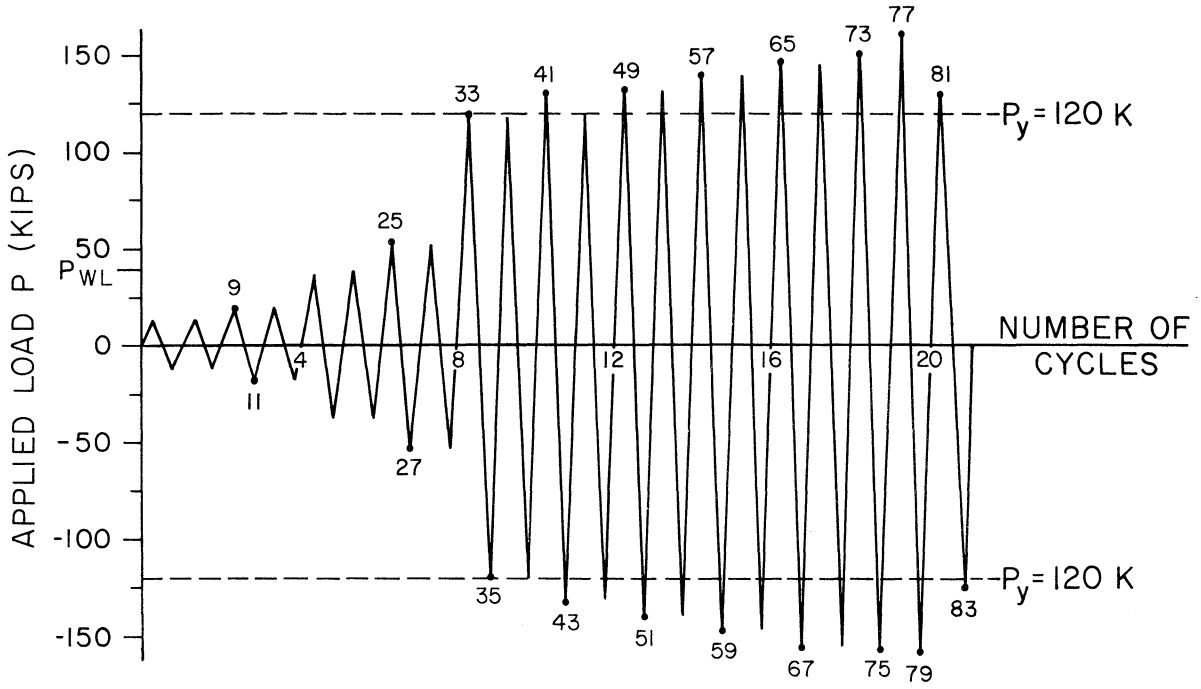

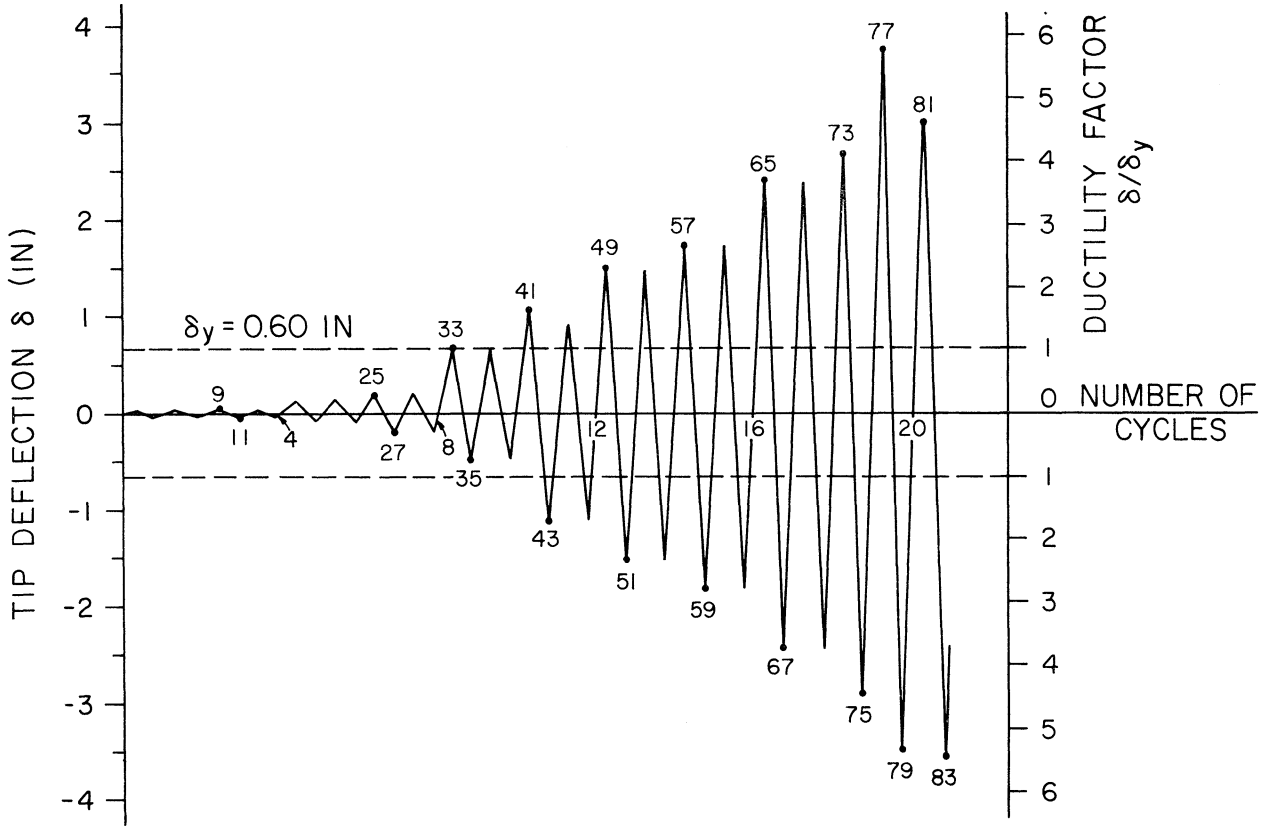

BEAM 43

FIG. 7 LOADING PROGRAM -- BEAM 43

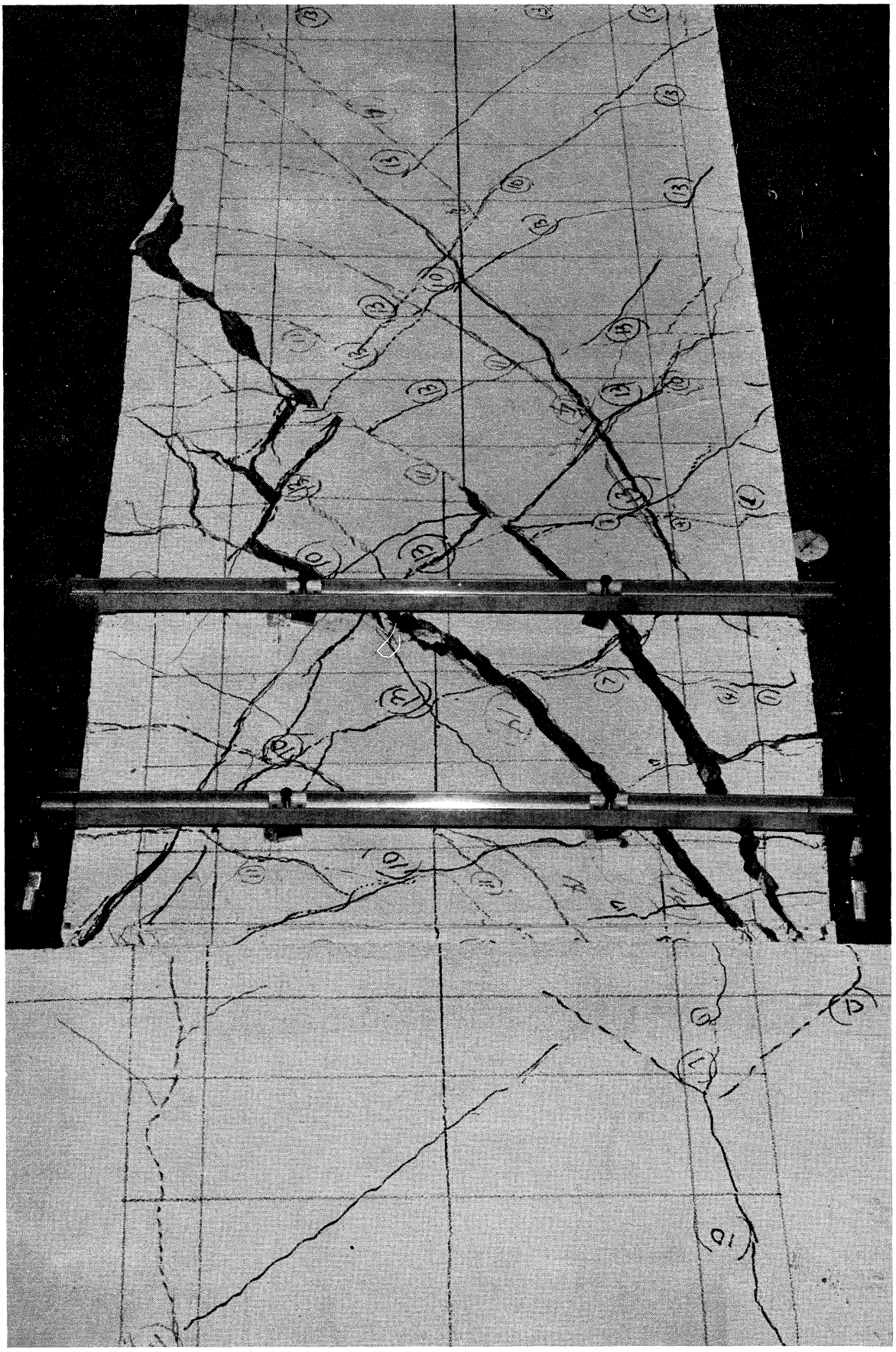

FIG. 8 BEAM 35 AFTER FAILURE

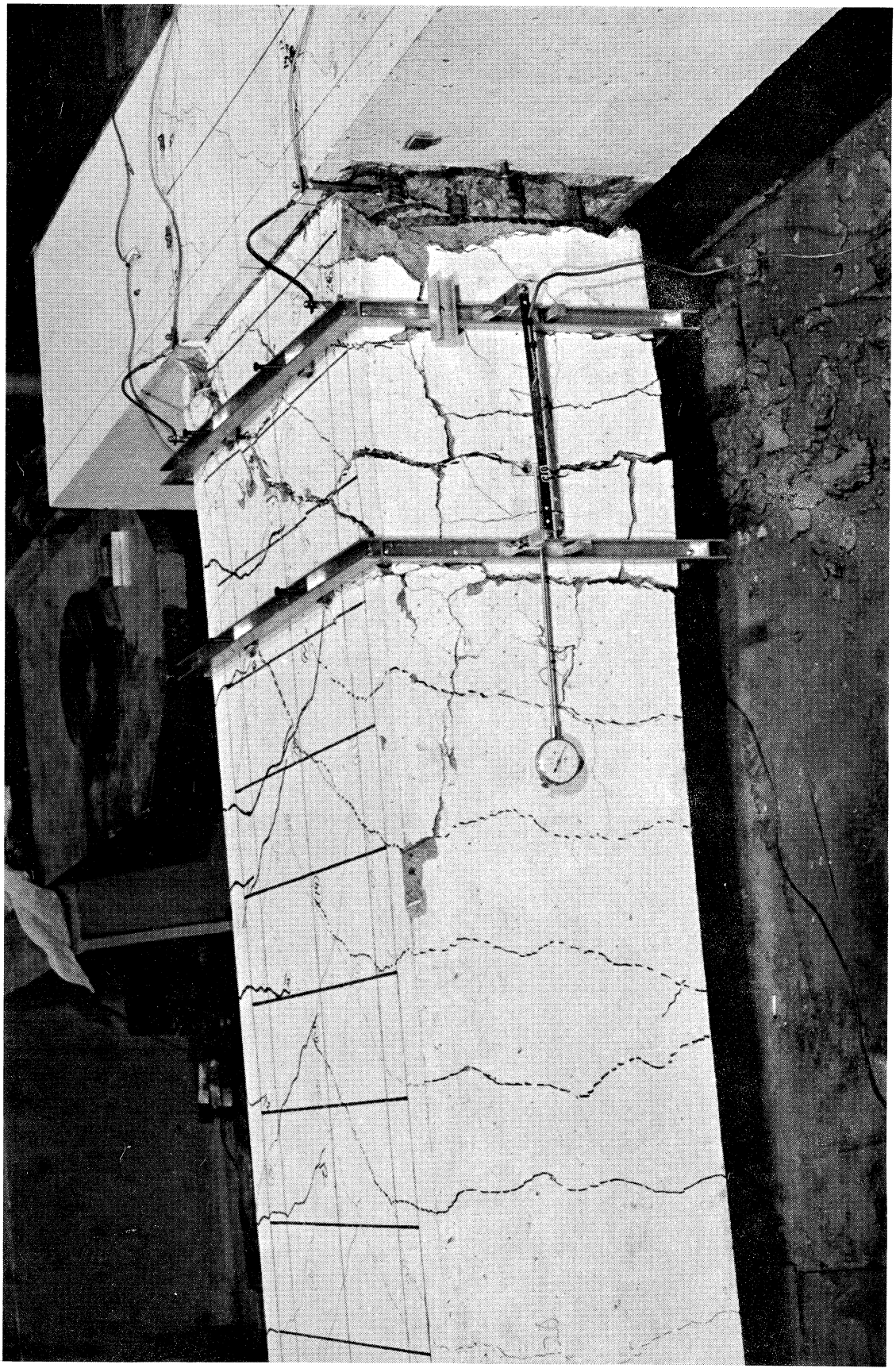

FIG. 9 BEAM 46 AFTER FAILURE

FIG. 10 BEAM 43 AFTER FAILURE

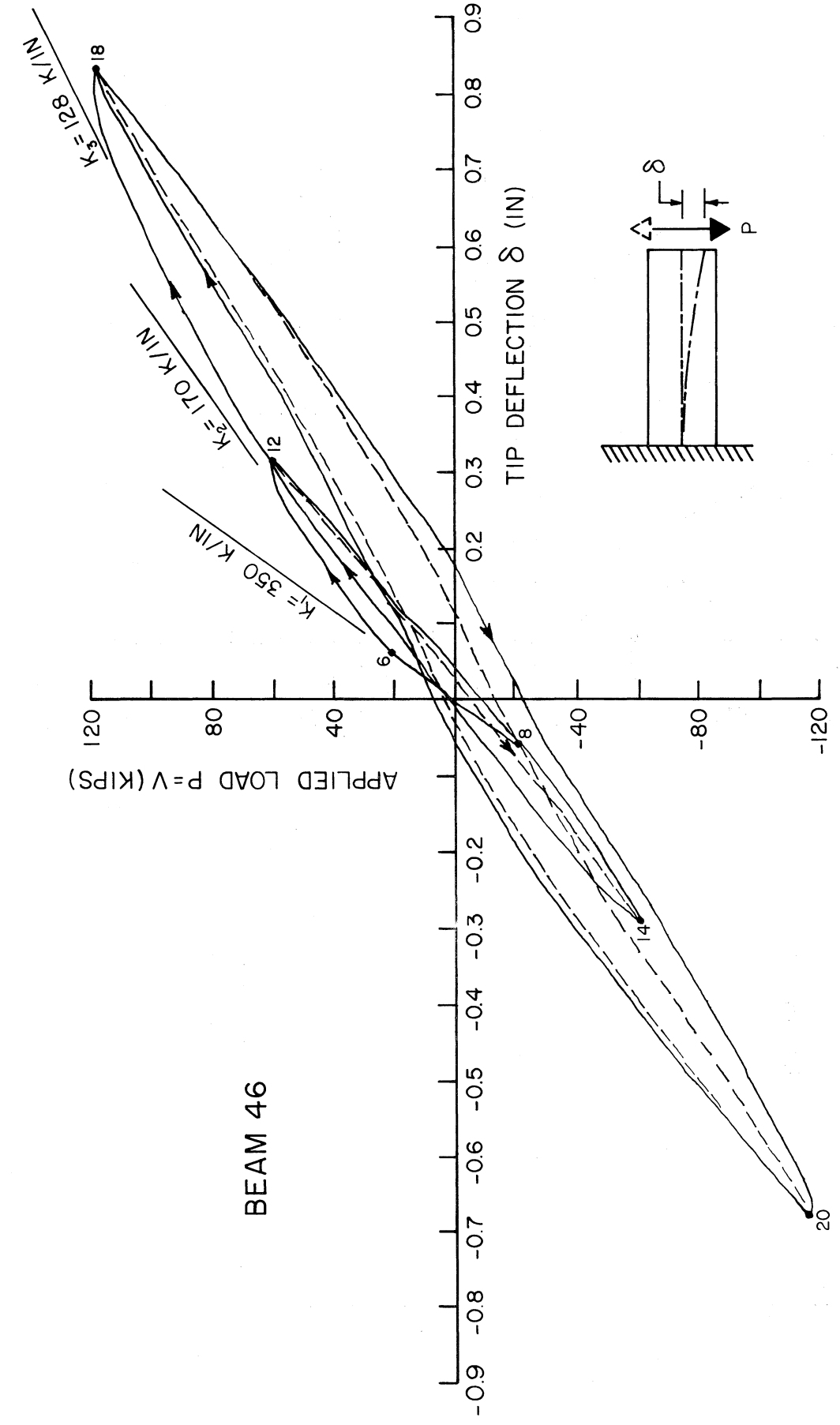

FIG. 11 P-δ DIAGRAM (UP TO YIELD) FOR BEAM 46

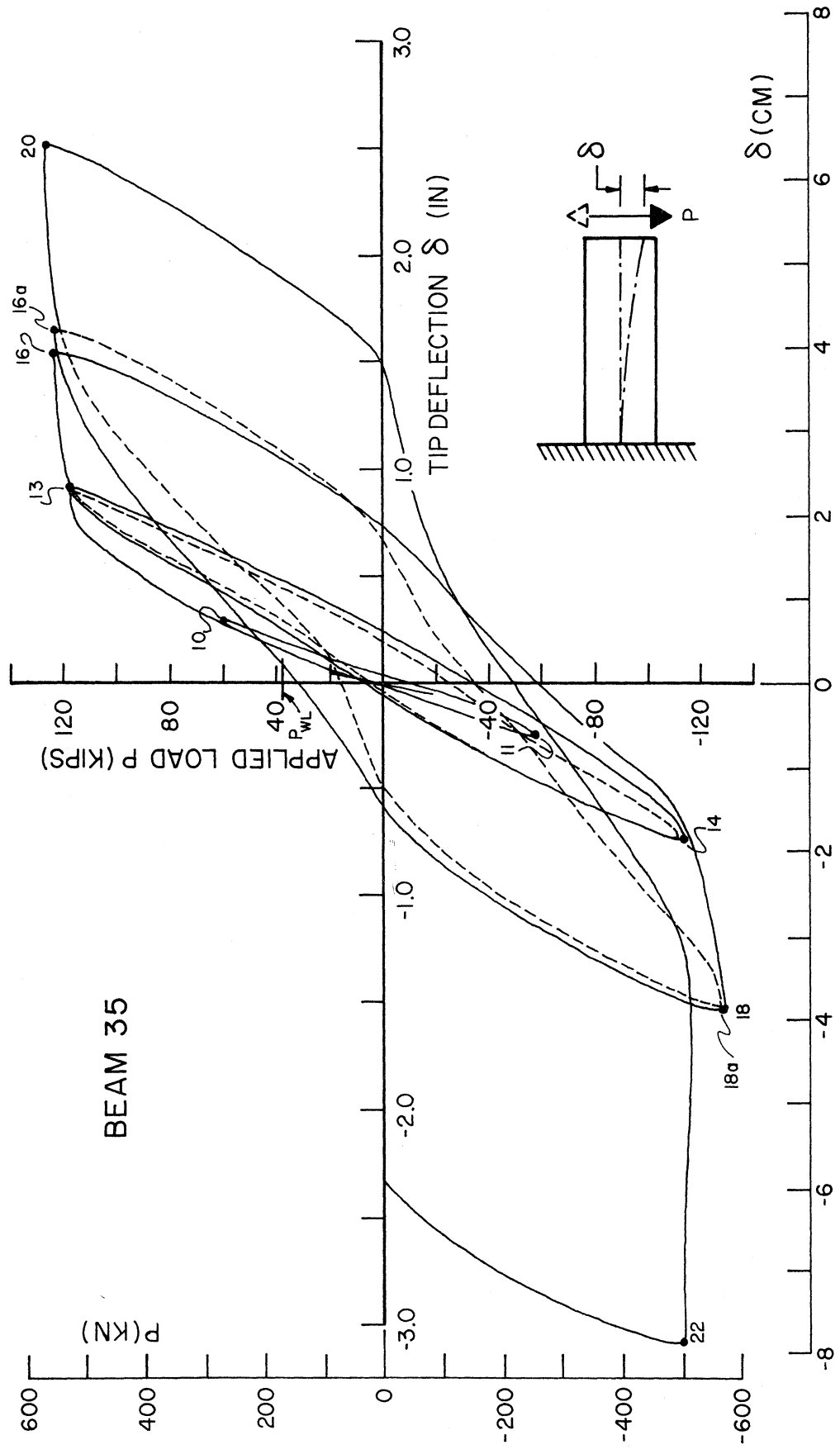

FIG. 12 P-δ DIAGRAM -- BEAM 35

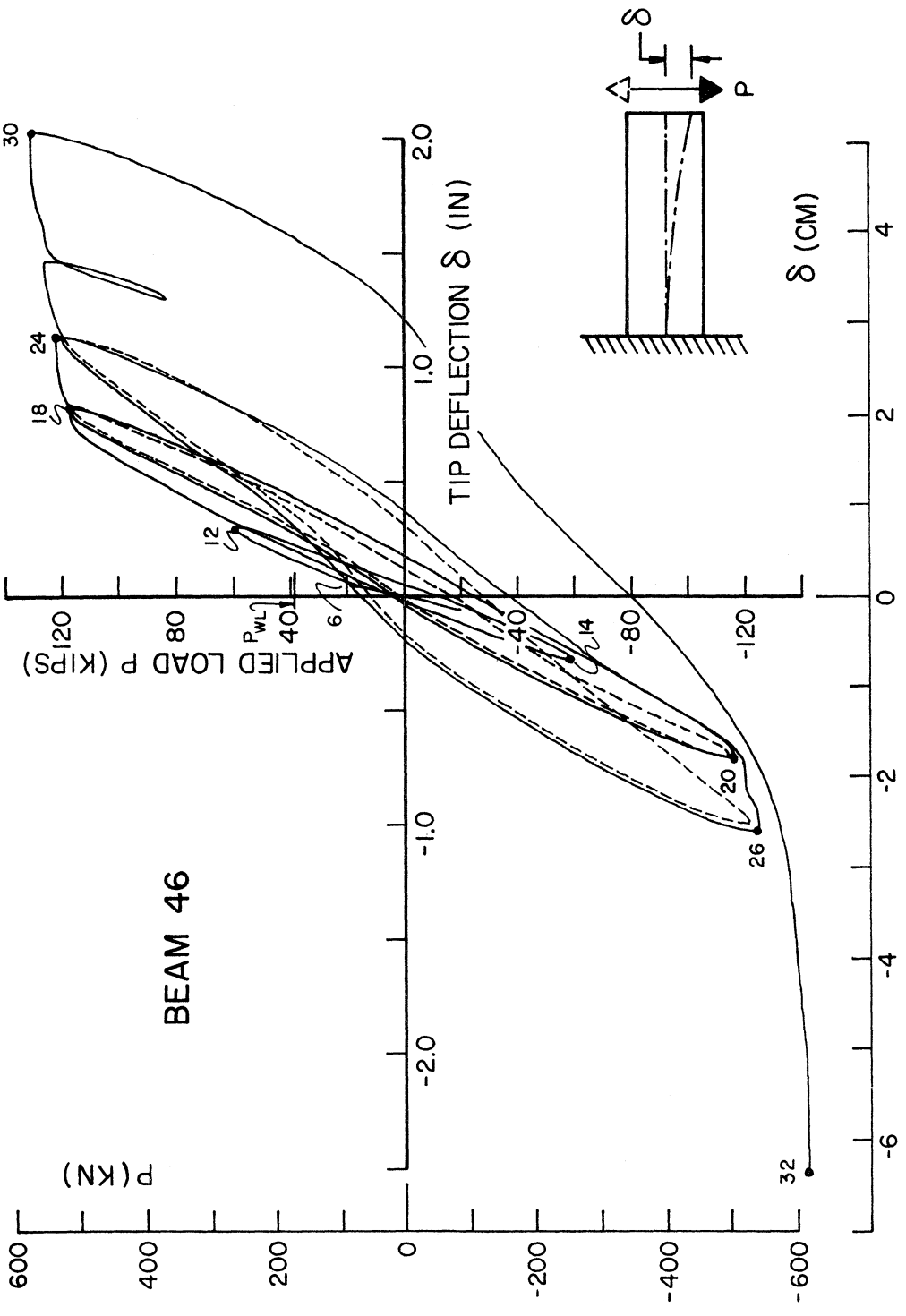

FIG. 13 P-δ DIAGRAM -- BEAM 46

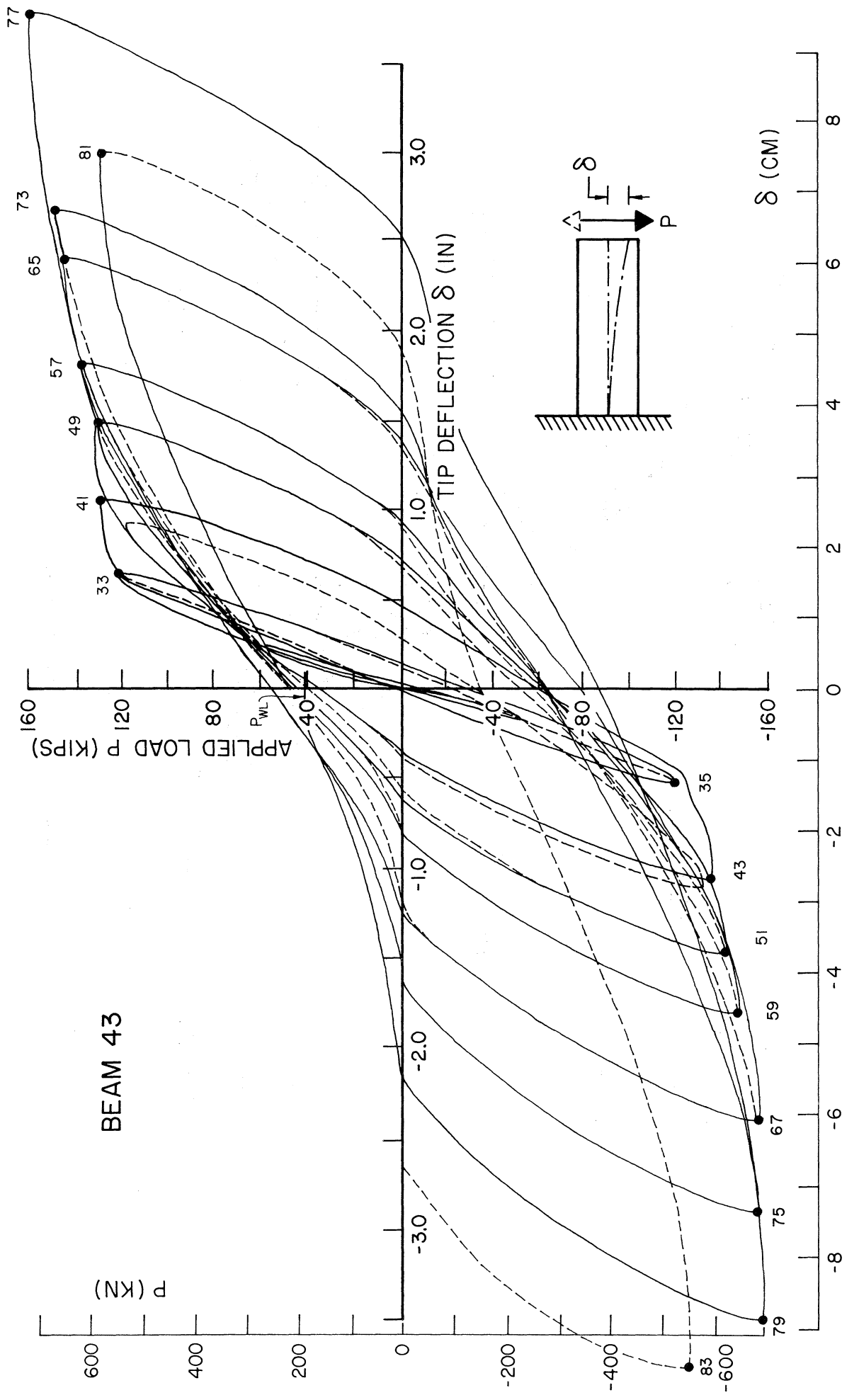

FIG. 14 P-δ DIAGRAM -- BEAM 43

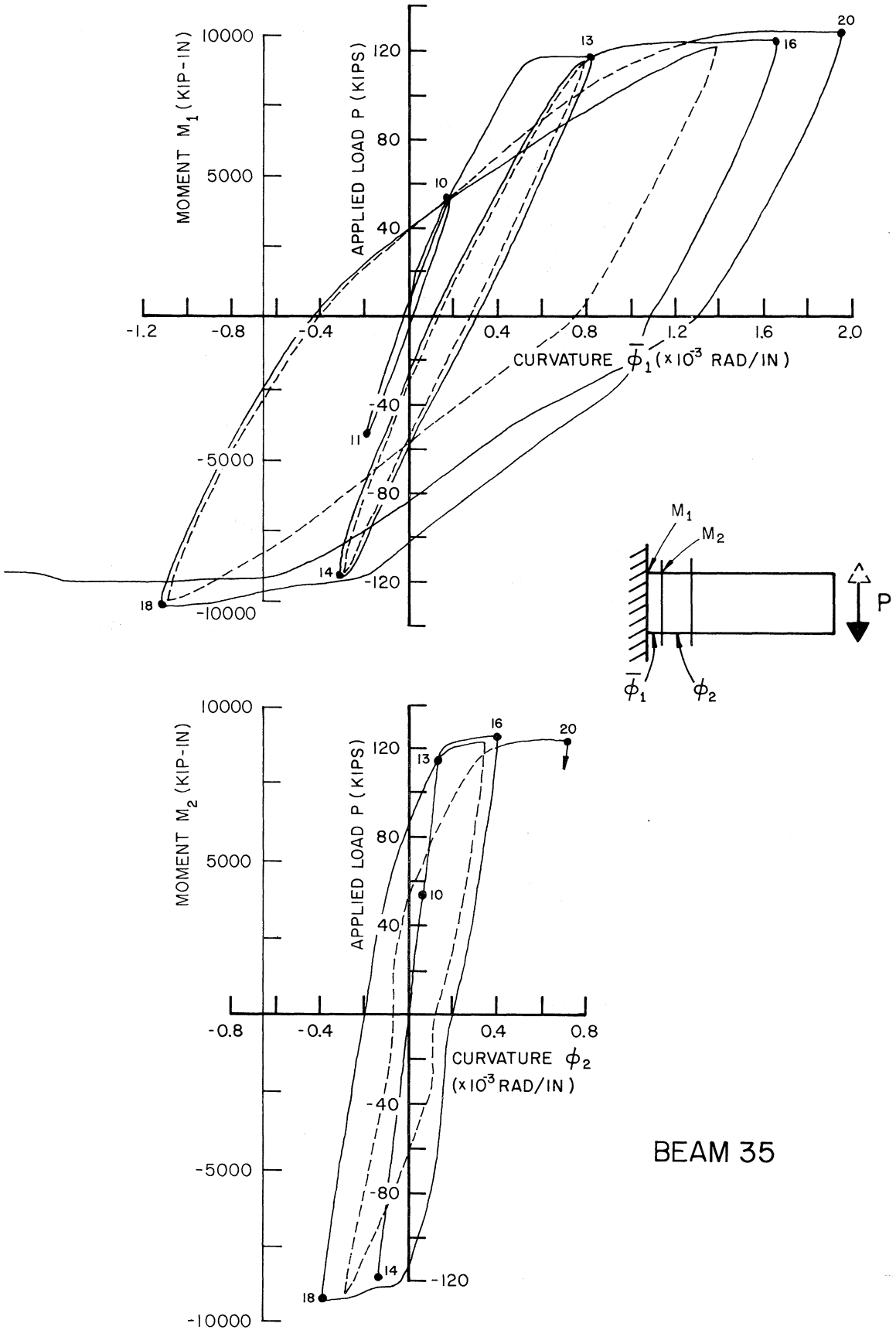

FIG. 15 M-Φ DIAGRAMS -- BEAM 35

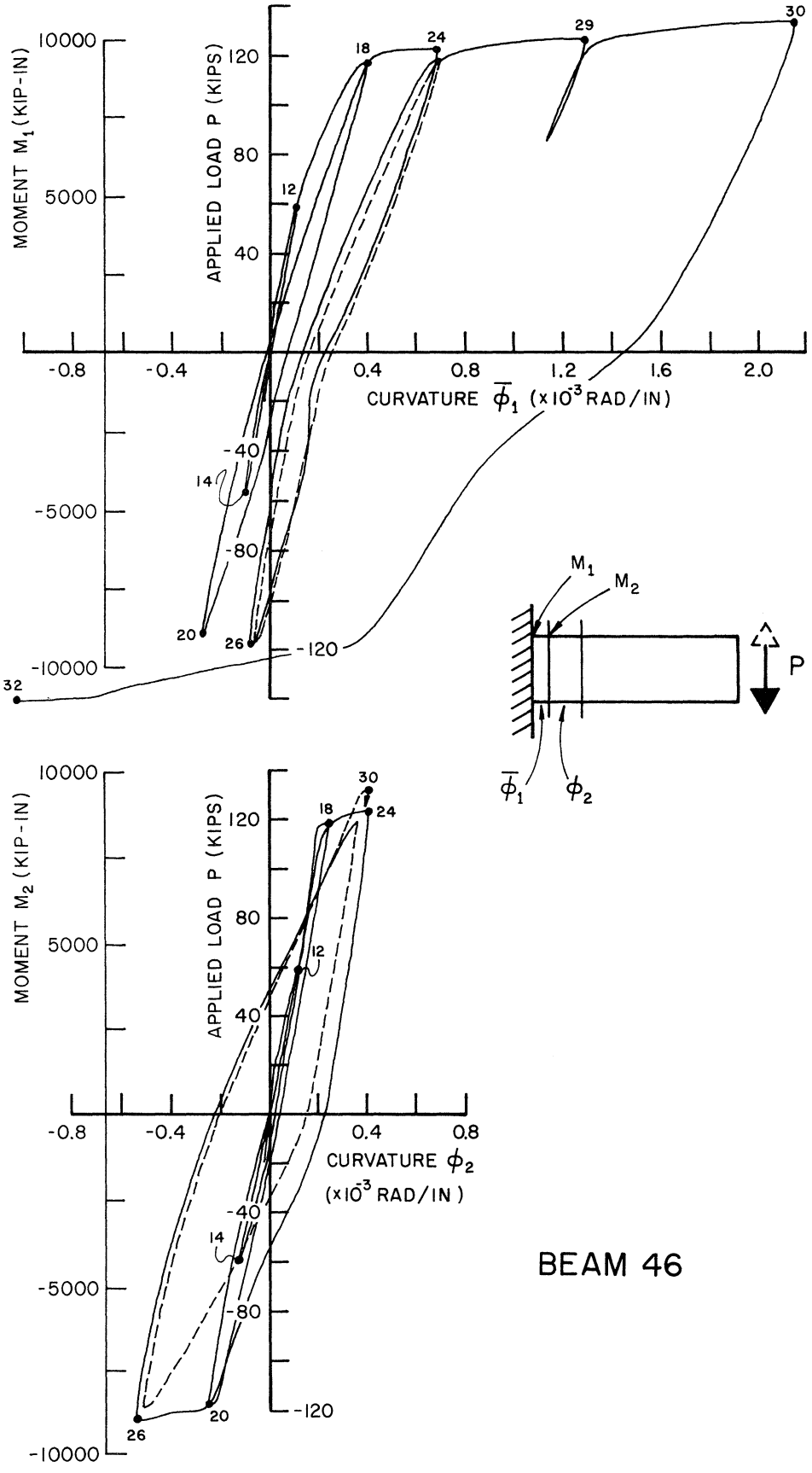

FIG. 16 M-Φ DIAGRAMS -- BEAM 46

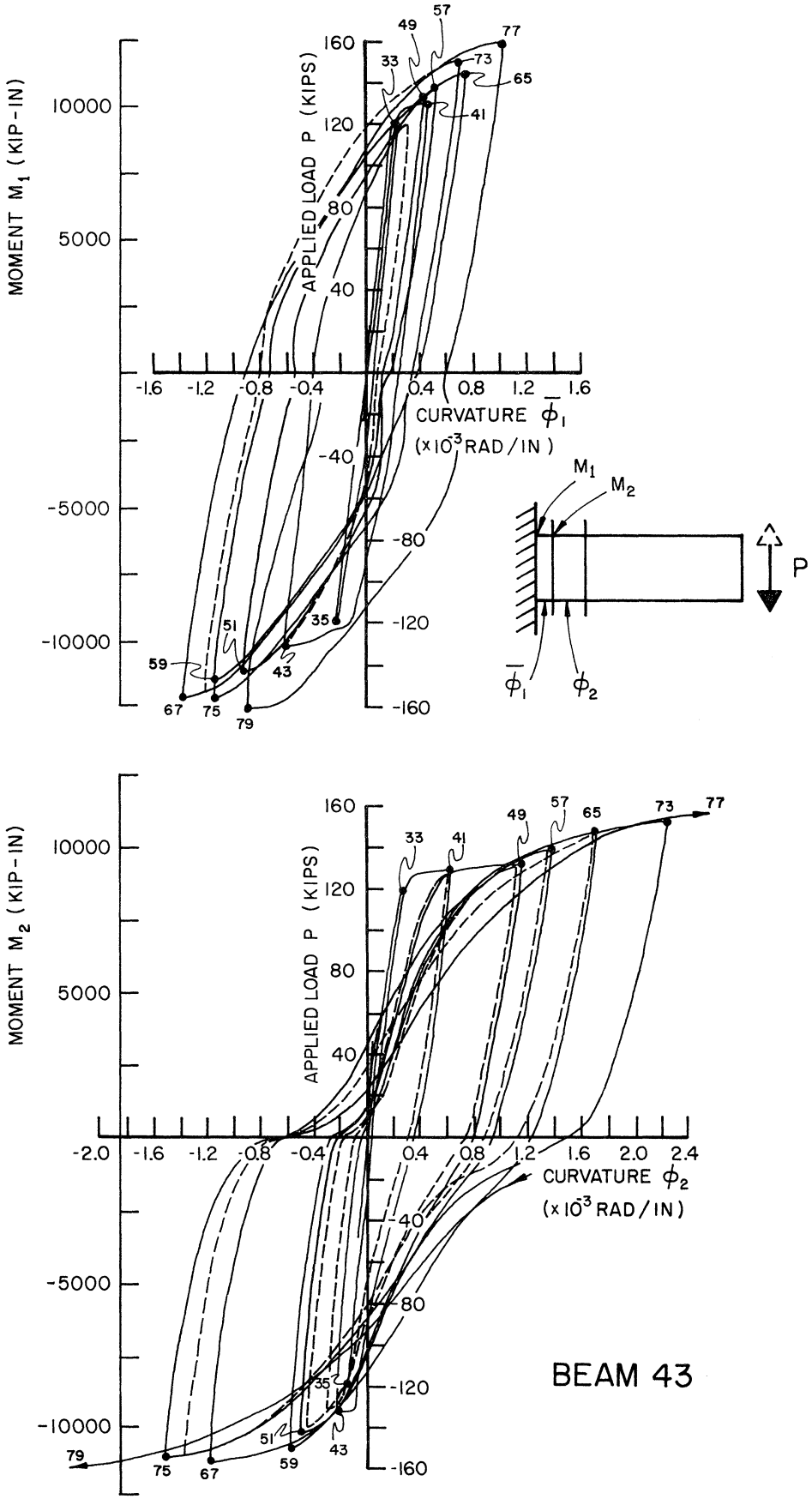

FIG. 17 M-Φ DIAGRAMS -- BEAM 43

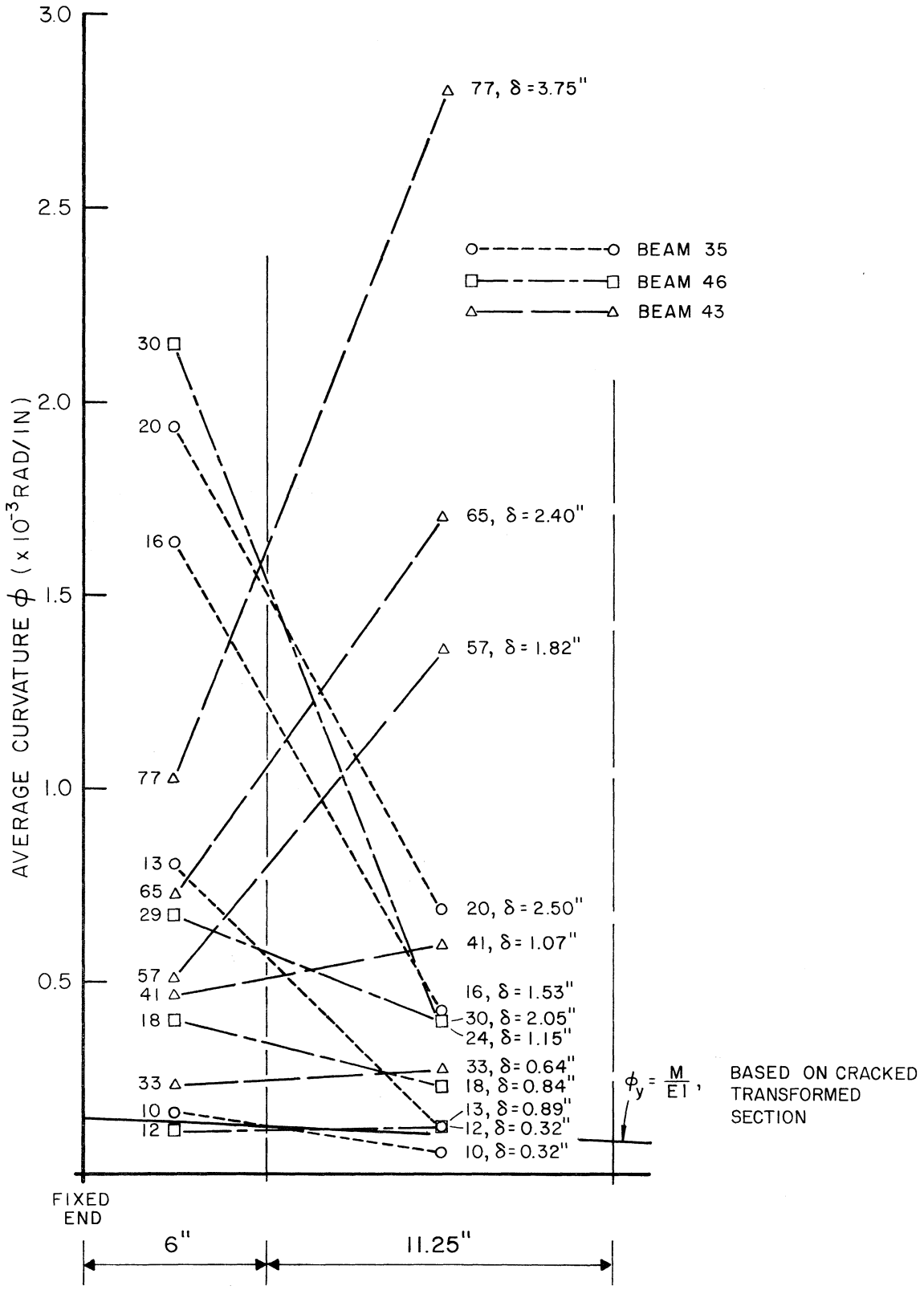

FIG. 18 MEASURED AVERAGE CURVATURES

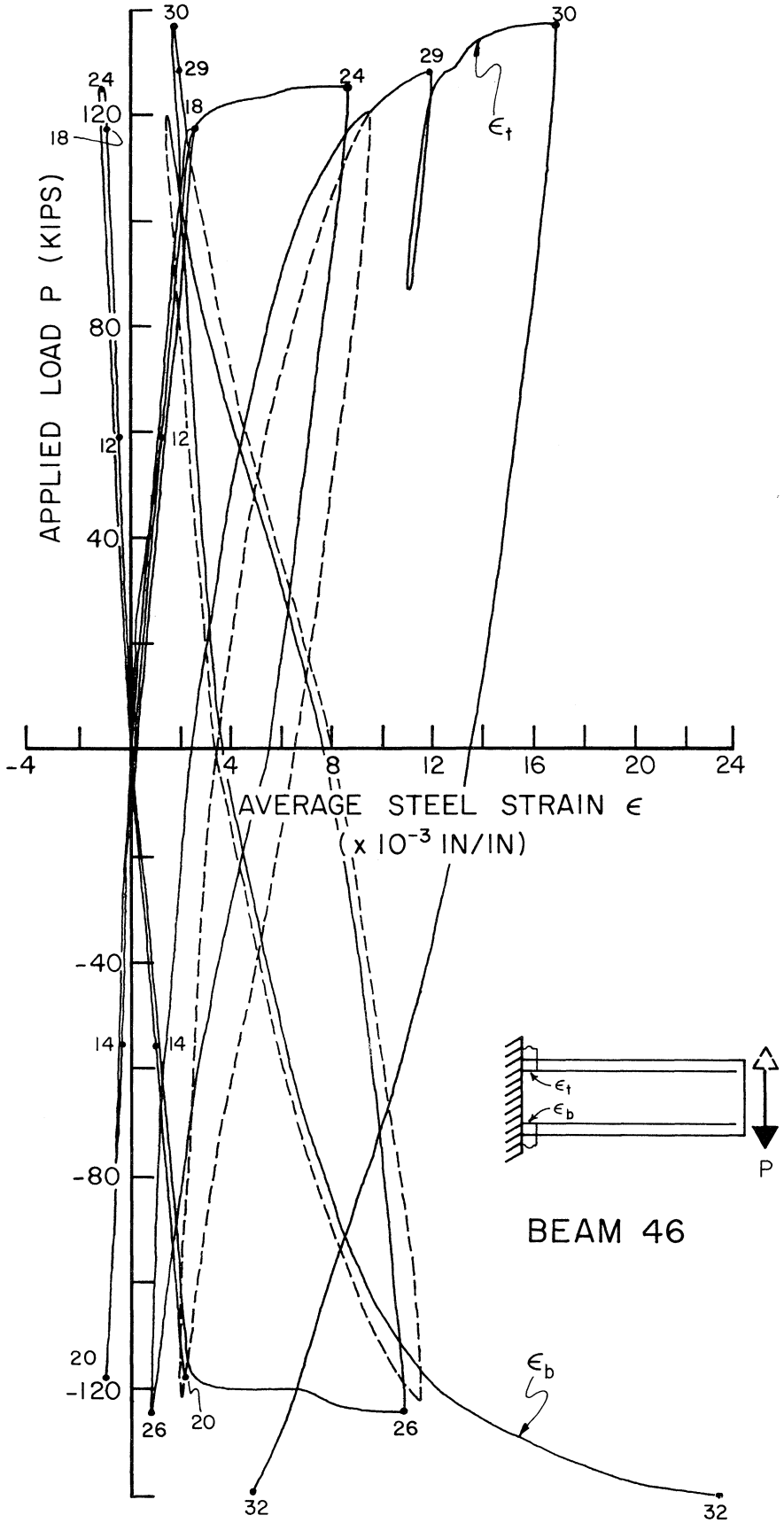

FIG. 19 AVERAGE STEEL STRAIN AT FIXED END -- BEAM 46

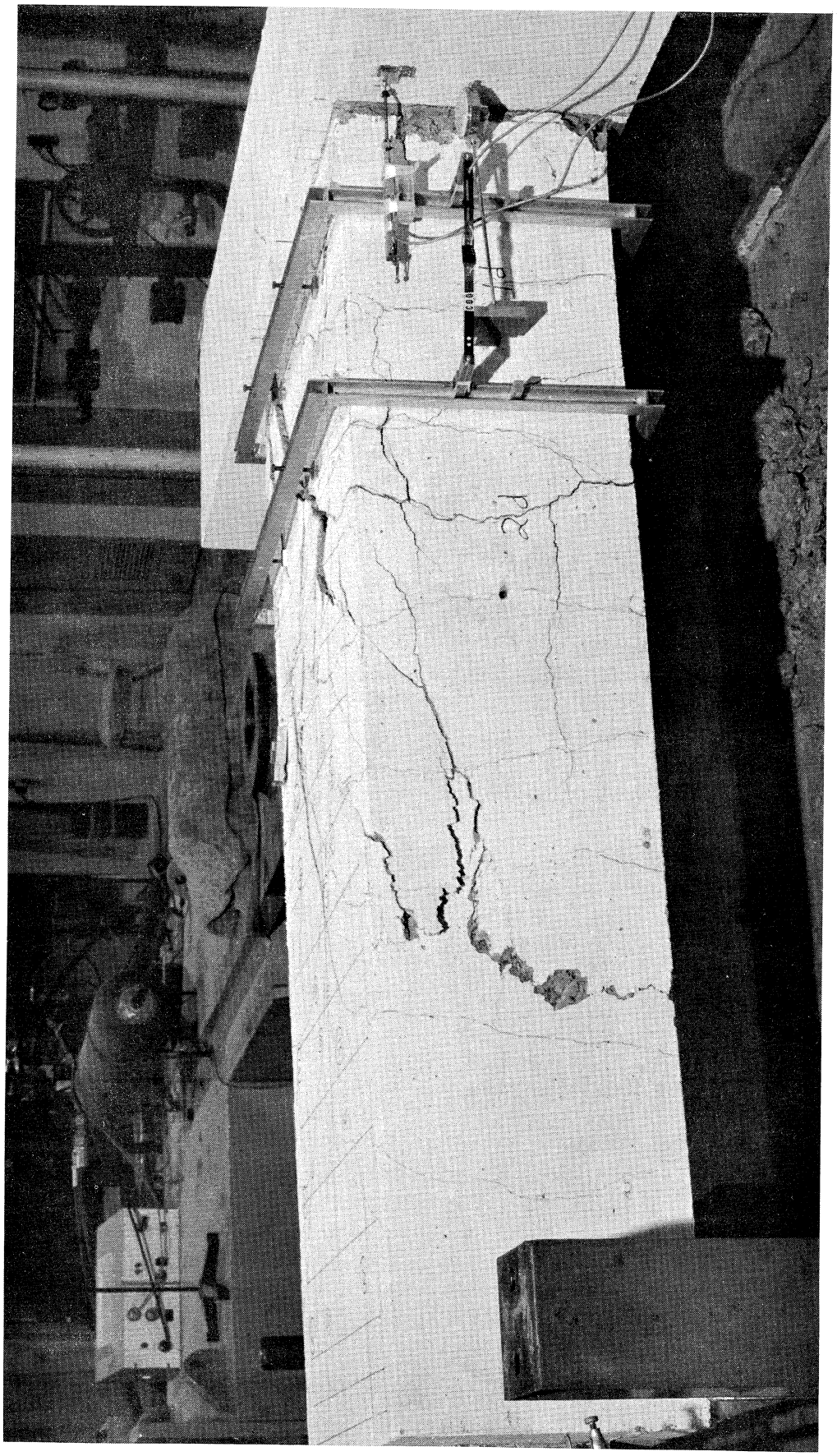

FIG. 20 SPLITTING OF CONCRETE COVER -- BEAM 35

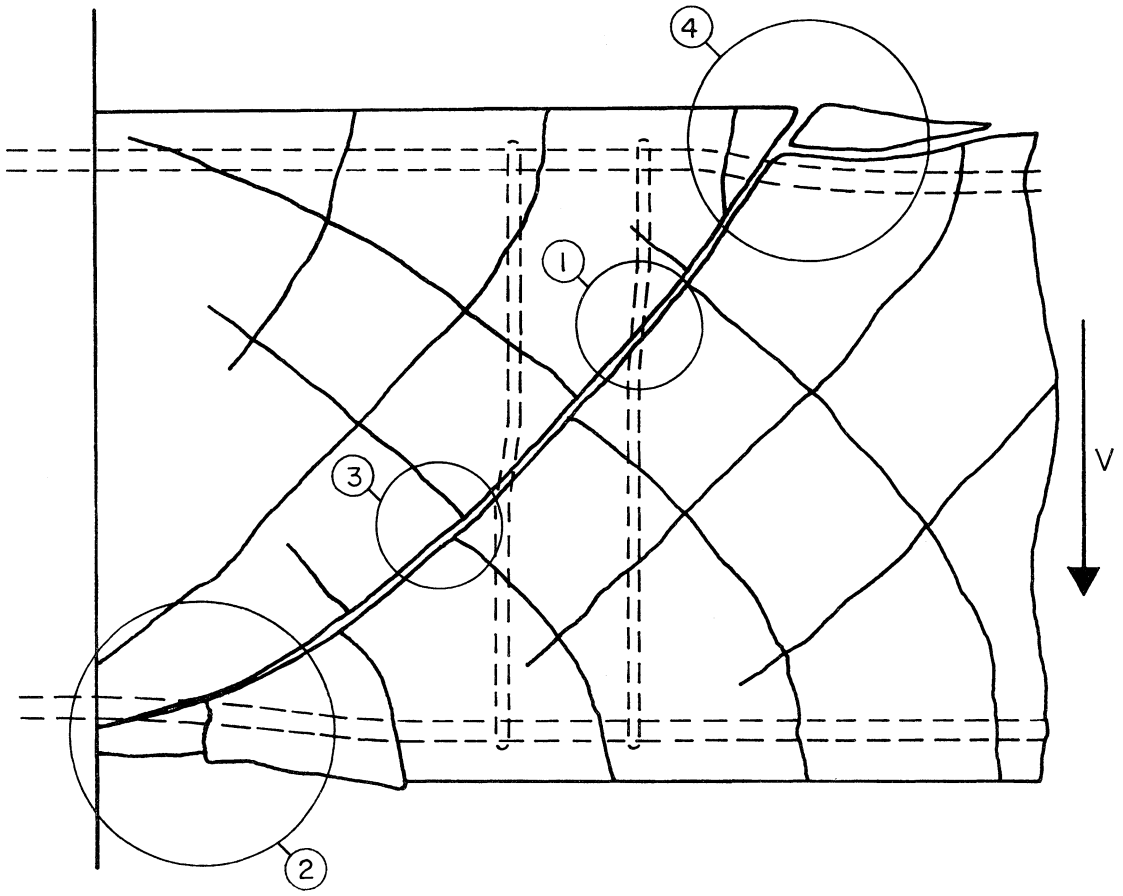

(1) DETERIORATED BOND AND POSSIBLY YIELDING OF STIRRUP TIES

(2) LESS EFFECTIVE COMPRESSION ZONE DUE TO PREVIOUS FLEXURAL CRACKING DURING LOAD REVERSALS

(3) DETERIORATED INTERLOCKING FORCE DUE TO ABRADED CONCRETE SURFACE AND YIELDING OF STIRRUP TIES (LESS CONFINEMENT OF CONCRETE)

(4) DOWEL ACTION, LOSS OF BOND AND SPLITTING OF CONCRETE COVER

FIG. 21 SHEAR FAILURE MECHANISM

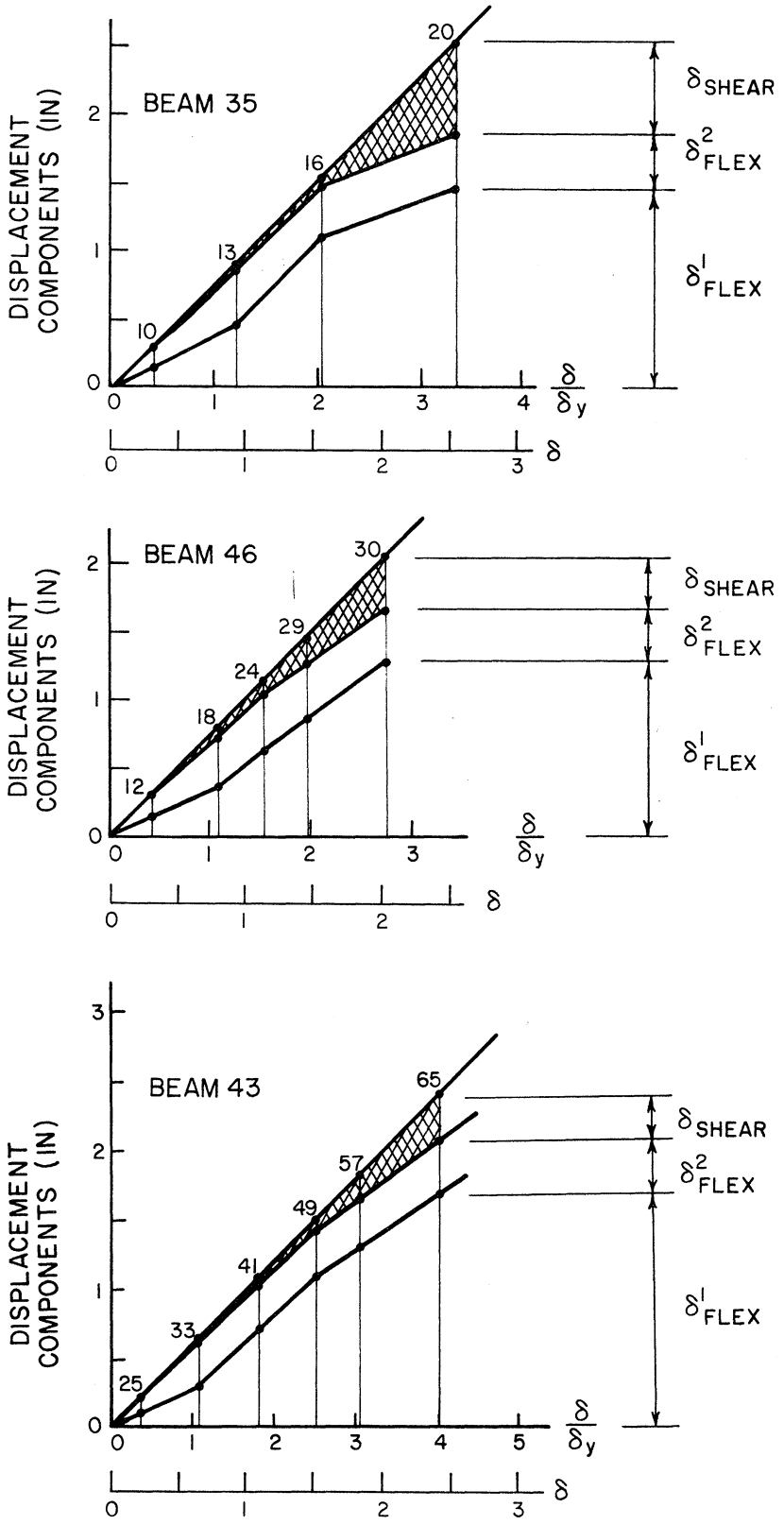

FIG. 22 ESTIMATE OF TIP DEFLECTION CAUSED BY SHEAR

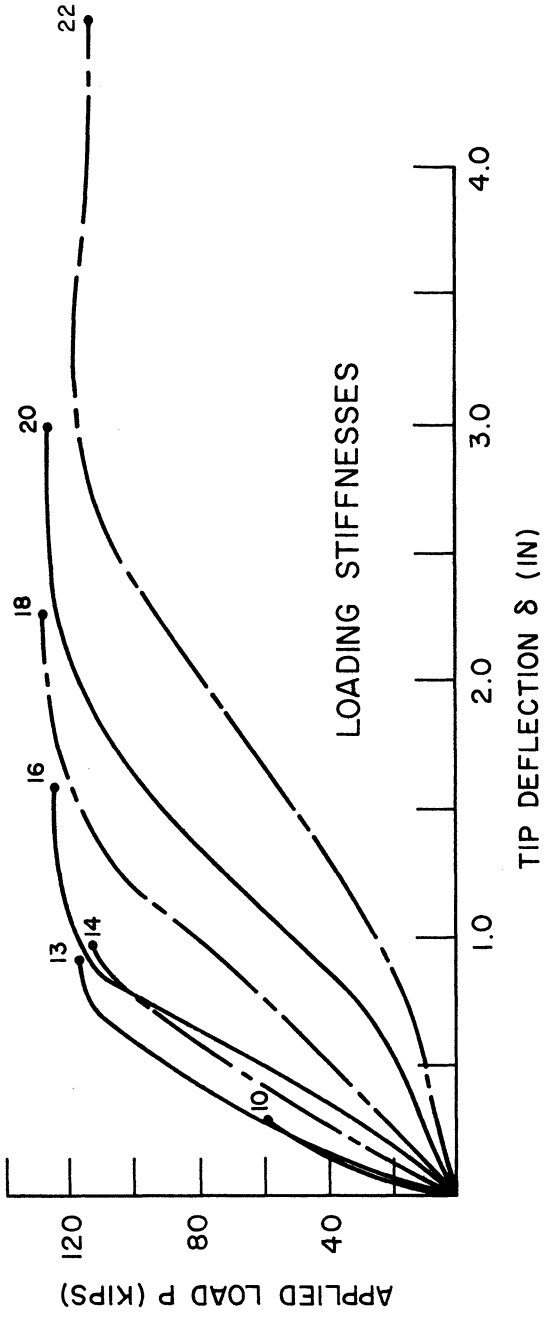

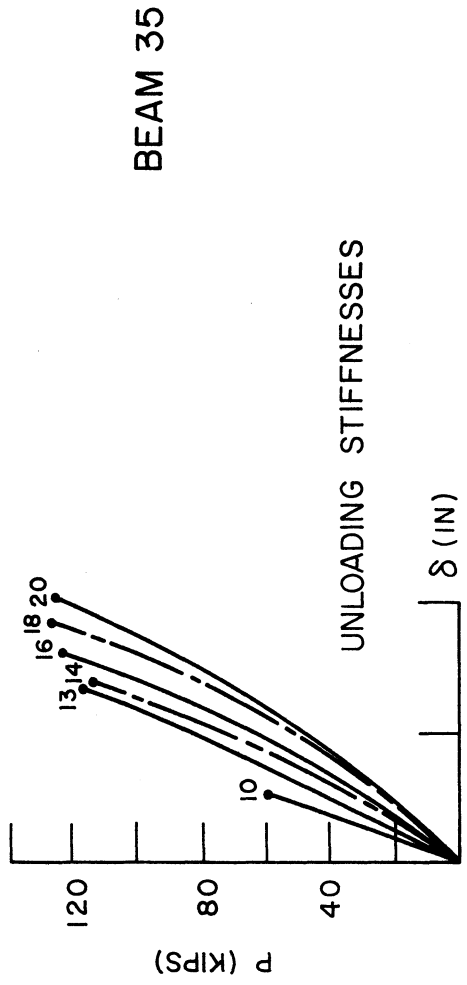

FIG. 23 DETERIORATION IN STIFFNESS -- BEAM 35

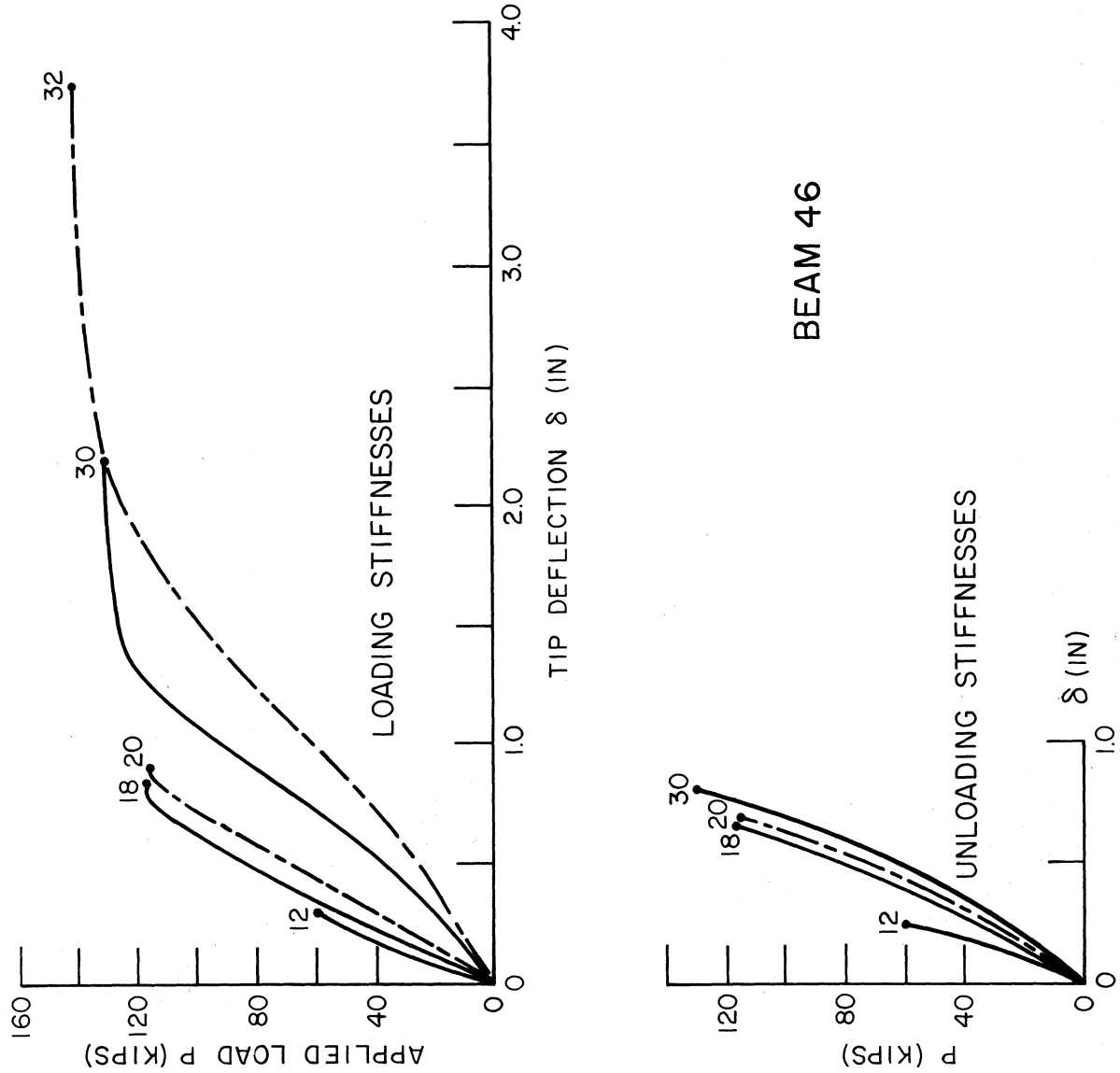

FIG. 24 DETERIORATION IN STIFFNESS -- BEAM 46

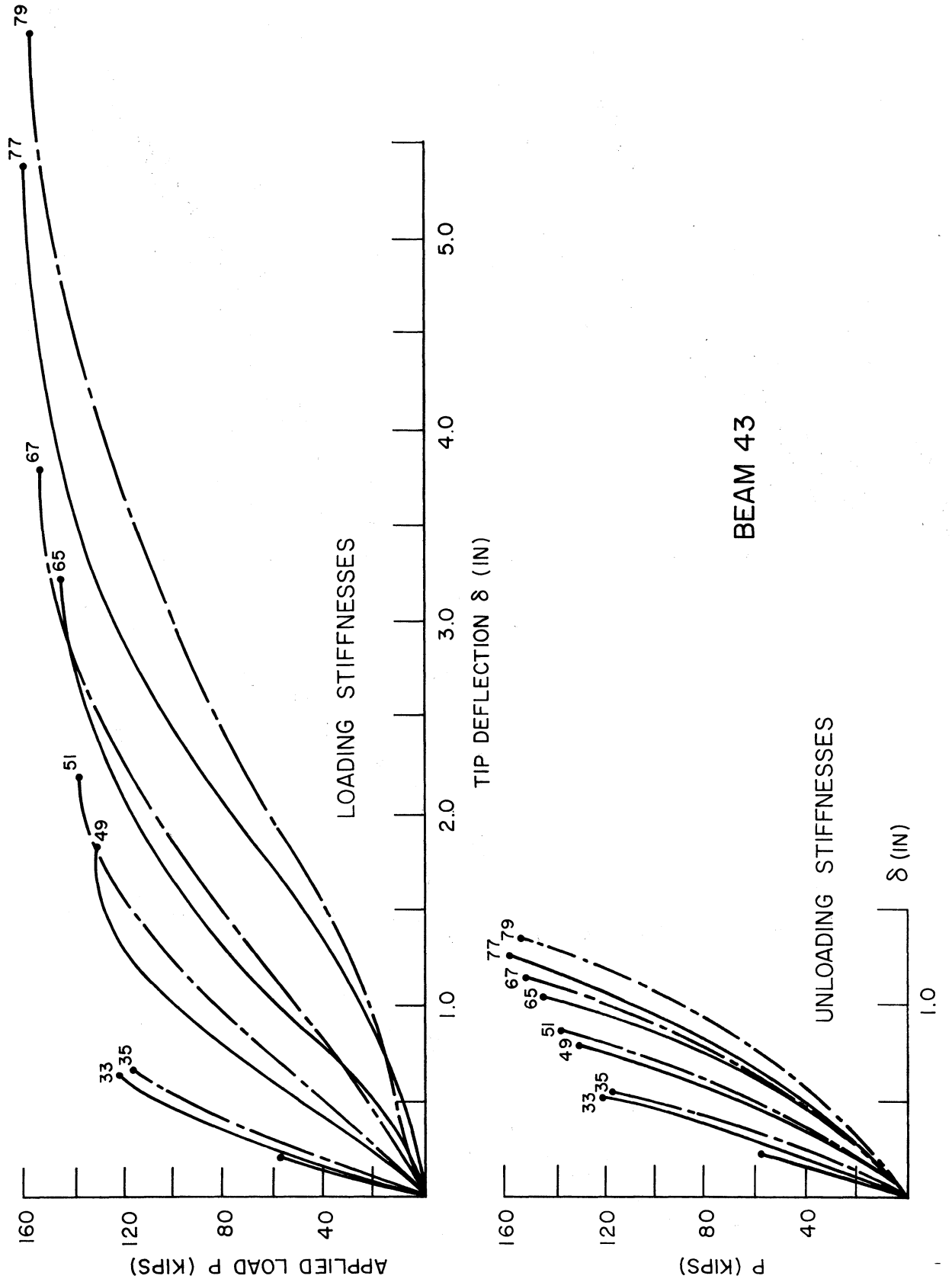

FIG. 25 DETERIORATION IN STIFFNESS -- BEAM 43

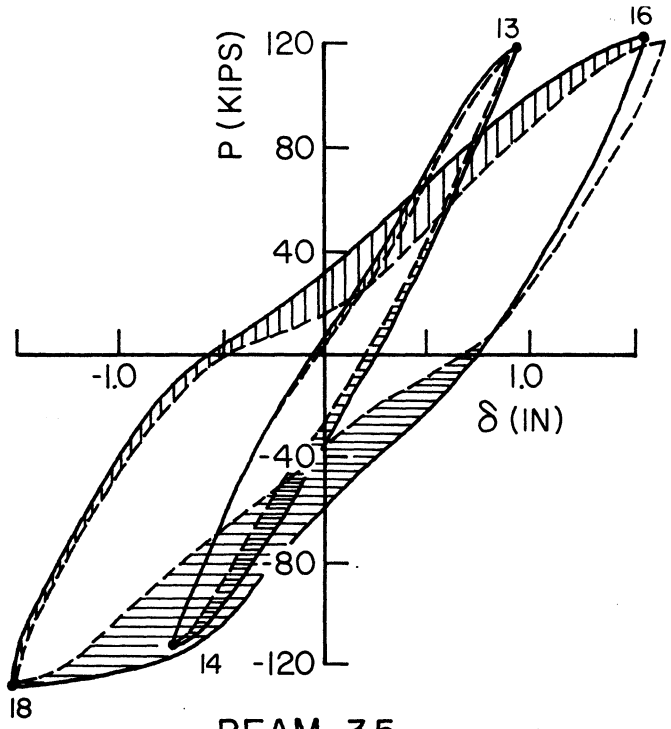

BEAM 35

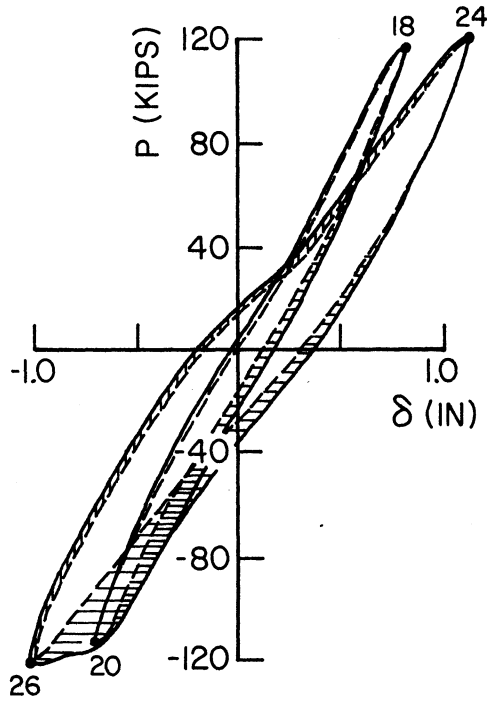

BEAM 46

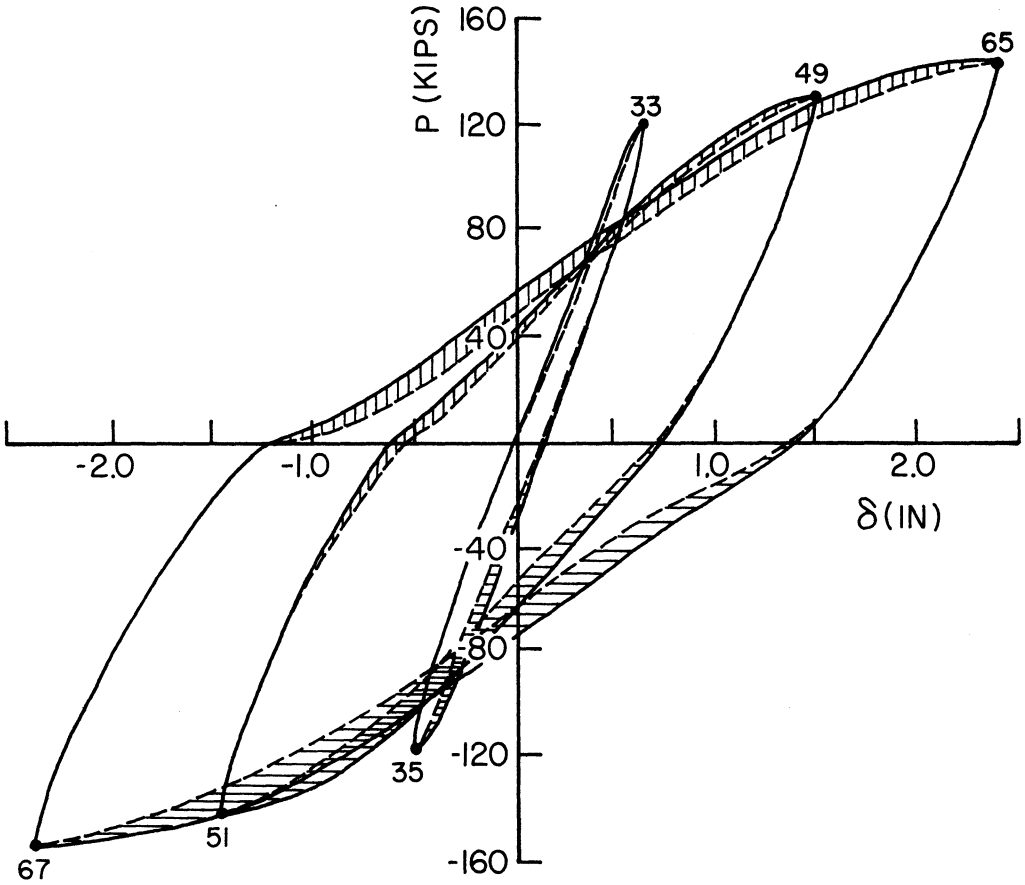

BEAM 43

FIG. 26 STIFFNESS DETERIORATION FROM FIRST TO SECOND CYCLE OF THE SAME DEFLECTION AMPLITUDE

APPENDIX A

MATERIALS AND FABRICATION

The concrete was made of Type II Portland Cement and Livermore Valley Aggregates of 3/4 in. maximum size. It was attempted to simulate the concrete generally used in local construction. Concrete batch quantities for one cubic yard as well as physical properties of the aggregate and details of compressive strength, tensile strength and modulus of rupture are presented in Tables A1 to A6. The strength data presented are average values obtained from several test specimens. Typical stress-strain diagrams for the concrete used in Beam 43 are shown in Fig. A1.

The tension and compression steel consisted of high strength deformed bars which conformed to ASTM designation for a 60 grade steel. The stress-strain diagrams for No. 9 bars of Beam 46 and Beam 43 are shown in Fig. A2. The No. 9 bars of Beam 35 came from the same heat as those of Beam 46 and exhibit almost identical strength characteristics.

The stirrups were specified to be of grade 40 steel, however, tension tests showed a yield strength of 60 ksi for the stirrups of Beams 46 and 43 and of 53 ksi for Beam 35.

The specimens were cast in place in plywood forms stiffened with wood battens. The concrete was compacted with a high frequency vibrator. After seven days the forms were removed. All beams and test cylinders were cured with wet sacks under plastic covering for seven days.

The experiments were carried out when the concrete attained the desired compression strength, which was 14 days (for Beams 35 and 43) and 28 days (for Beam 46), respectively, after casting.

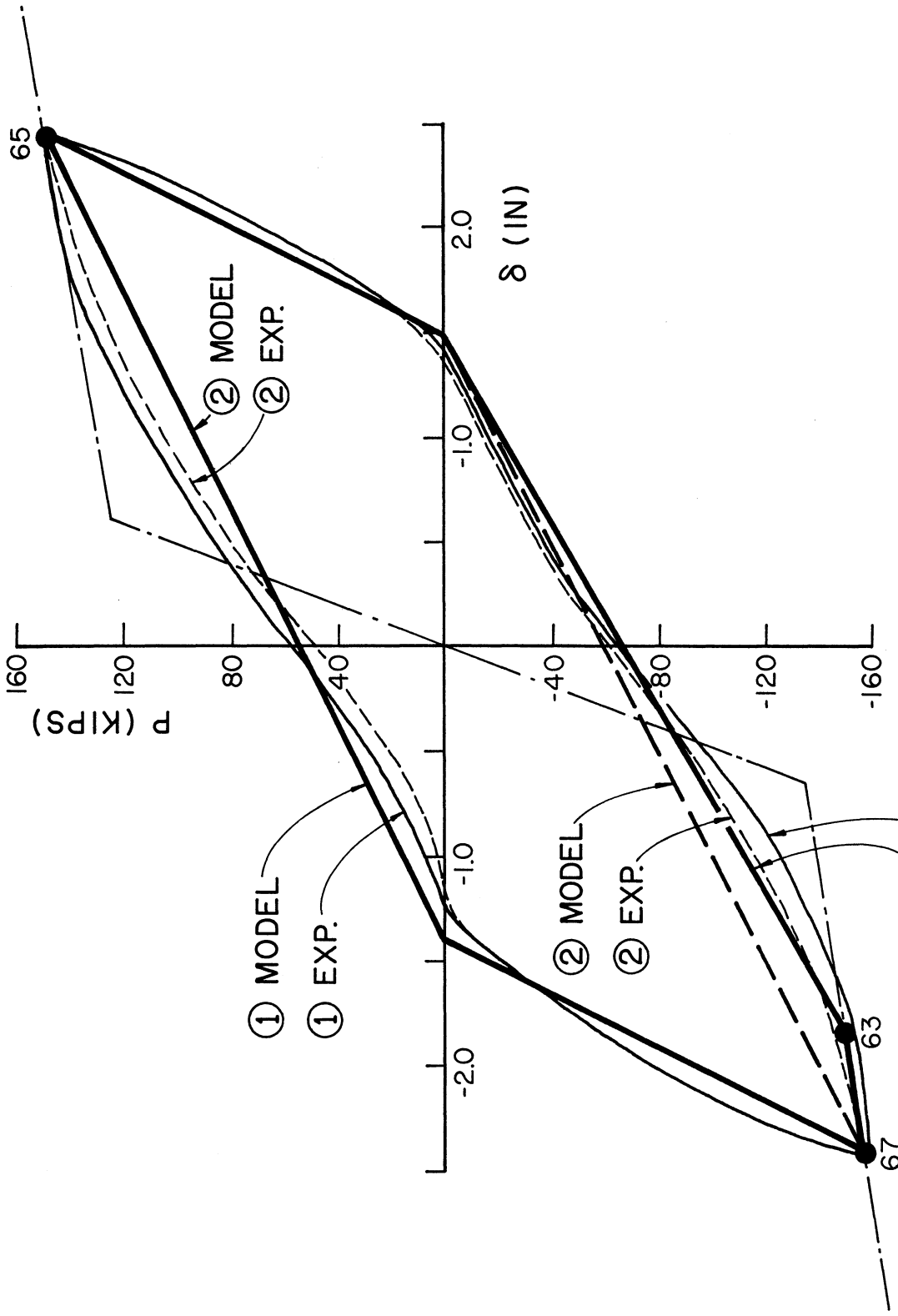

FIG. 27 COMPARISON OF EXPERIMENTAL LOOPS WITH PROPOSED HYSTERESIS MODEL

TABLE A1. CONCRETE BATCH QUANTITIES FOR ONE CUBIC YARD SATURATED SURFACE-DRY AGGREGATES

Material	Quantities for 1 cu. yd. (lbs.)		
	Beam 35	Beam 46	Beam 43
Type II cement	614	533	752
Water	313	307	308
Fine aggregate	1504	1531	1355
Coarse Aggregate (3/4" x 1/4")	1621	1595	1597
Total	4052	3966	4012

TABLE A2. PHYSICAL PROPERTIES AND GRADATION OF AGGREGATES. (Livermore Valley Aggregate which is predominantely Graywake)

Property	Fine Eliot Sand	Coarse Eliot 3/4" x 1/4"
Bulk Sp.G. (SSD Basis)	2.65	2.69
Dry Rodded wf.pcf.		102
Absorption Capacity OD to SSD.	1.40	1.50
Absorption AD to SSD.	1.00	0.90

TABLE A3. SIEVE ANALYSIS

U.S. Standard Sieve Size	Cumulative Percent Retained	
	Fine	Coarse
1.5"		
1.0"		0
3/4"		7
1/2"		42
3/8"		69
4	0	98
8	13	99
16	43	100
30	70	100
50	89	100
100	97	100
200	100	100
Fineness Modulus	3.12	7.73

TABLE A4. SPLITTING TENSILE STRENGTH DATA

Specimen	Age days	Diam. in.	Length in.	Max. Load lb.	Splitting T. Strength psi
Beam 35	14	6.00	12.0	41000	$363=5.8\sqrt{f'_c}$
Beam 46	30	5.97	12.0	51000	$450=7.1\sqrt{f'_c}$
Beam 43	14	6.00	12.0	55300	$490=6.9\sqrt{f'_c}$

TABLE A5. COMPRESSIVE STRENGTH DATA

Specimen	Age days	Area in^2	Max. Load lb.	Compress. Strength psi.
Beam 35	7	28.09	78000	2780
	14	28.00	108000	3860
Beam 46	14	28.09	80000	2850
	28	28.00	112000	3990
Beam 43	7	28.00	112200	3990
	14	28.00	141000	5030

TABLE A6. MODULUS OF RUPTURE

Specimen	b in.	d in.	Span in.	Load lb.	Mod. of Rupture psi.
Beam 35	4.95	6.10	18.0	5260	$545=8.8\sqrt{f'_c}$
Beam 46	4.87	5.98	18.0	5905	$610=9.6\sqrt{f'_c}$
Beam 43	5.00	6.00	18.0	6025	$624=8.8\sqrt{f'_c}$

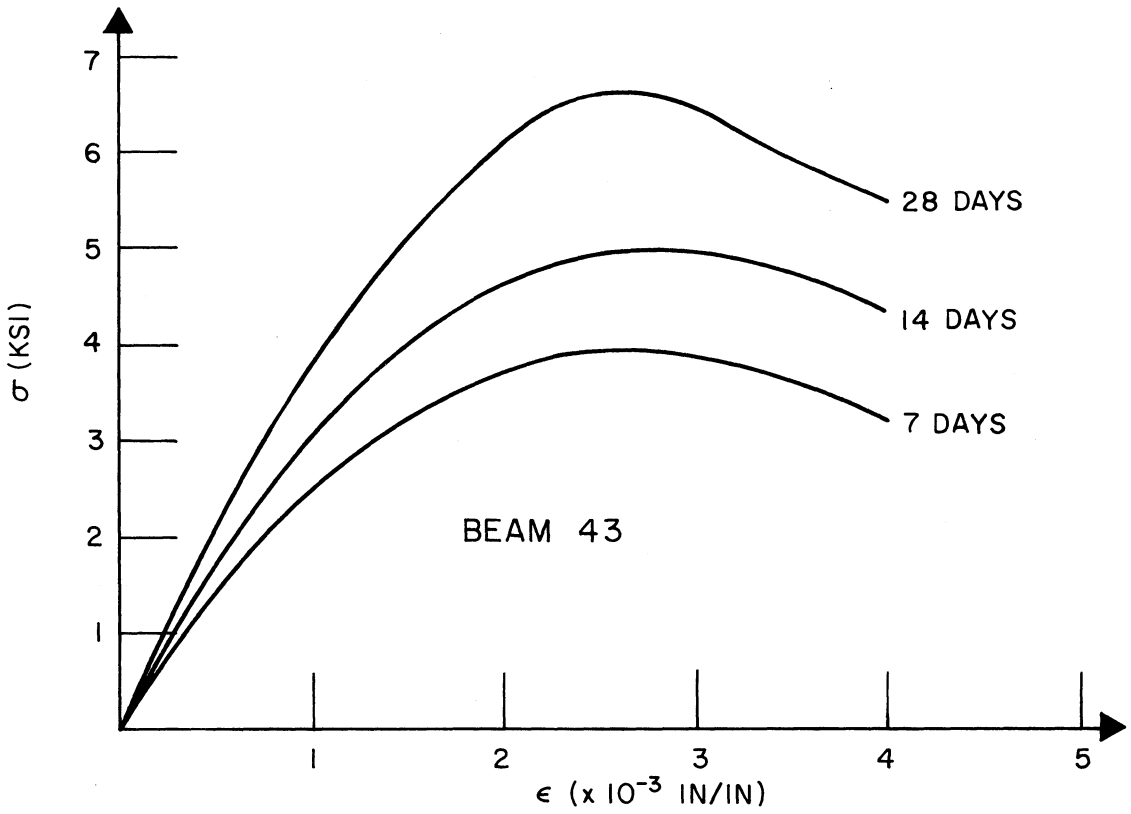

FIG. A1 σ-ε DIAGRAM FOR CONCRETE

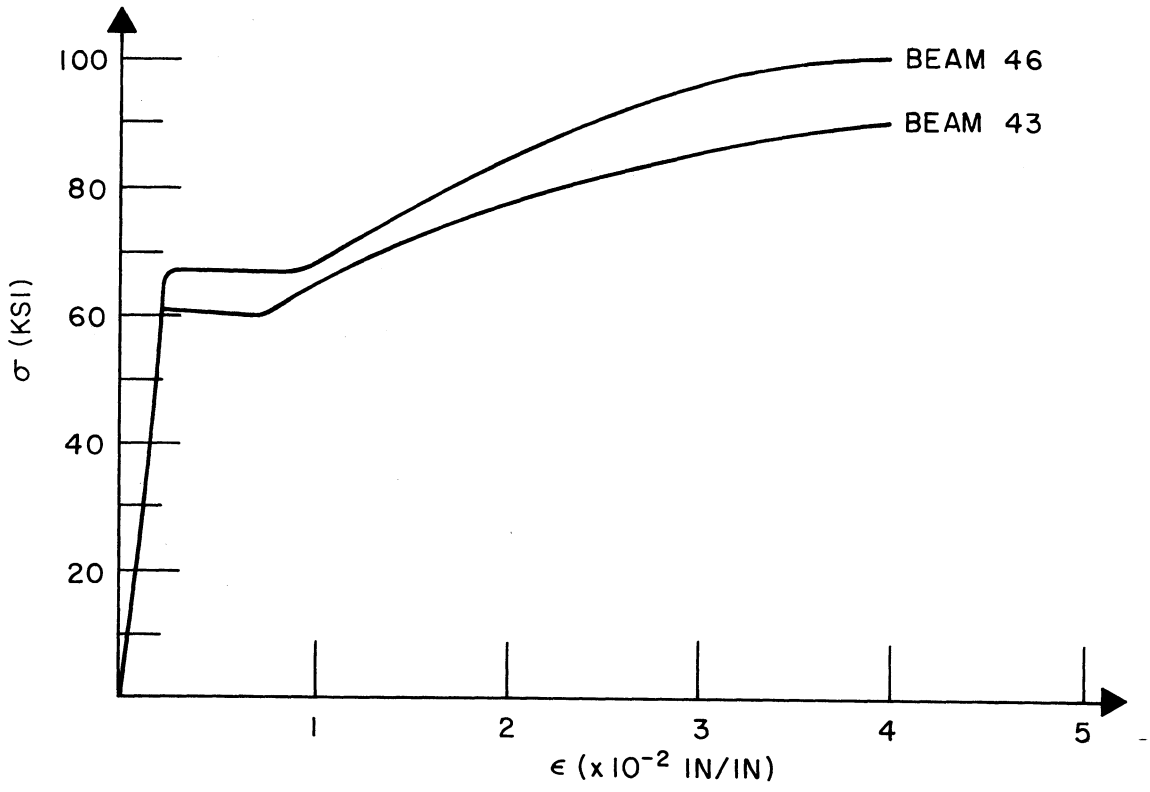

FIG. A2 σ-ε DIAGRAM FOR REINFORCING STEEL

APPENDIX B

COMPUTED STRENGTH OF SPECIMENS

The ACI - 63 Code [10] and the ACI - 71 Code [2] as well as Reference 1 were taken as bases for the design and the strength predictions of the three specimens. The capacity reduction factor ϕ as used in the two codes is ignored, i.e. ϕ is taken equal to one.

The specimen properties used in the following computations are summarized in Table 1 of this report.

Beam 35:

This beam was designed following the ACI - 63 Code. The limitation on the amount of longitudinal reinforcing steel is $p < 0.75\ p_b$. The compression steel was neglected in the computation of p_b since it was not expected to yield at ultimate strength according to Eq. (16-4) in Reference 10. The ratio p_b is then given by

$$p_b = \frac{0.85\ k_1\ f'_c}{f_y}\ \frac{87000}{87000 + f_y}$$

With k_1 equal to 0.85 this ratio becomes

$$p_b = 0.0235$$

and

$$0.75\ p_b = 0.0176 > p = 0.0158$$

When the effect of the compression steel is neglected, the ultimate design resisting moment is:

$$M_u = bd^2 f'_c \, q \, (1-0.59q)$$

where

$$q = p \frac{f_y}{f'_c}$$

With the actual yield strength of the steel used, one obtains

$$M_u = 8600 \text{ kip-in}$$

and

$$V_u = \frac{M_u}{\ell} = 110.2 \text{ kips}$$

DESIGN OF SHEAR REINFORCEMENT:

The shear taken by the concrete is

$$V_c = bd\left(1.9\sqrt{f'_c} + 2500p \frac{V_u d}{M_u}\right) = 49.5 \text{ kips} \leq 3.5\sqrt{f'_c}\, bd$$

Hence $V_s = V_u - V_c = 60.7$ kips has to be taken by web reinforcement. Taking #3 stirrup-ties with $f_y = 53$ ksi, the required spacing is

$$s = \frac{A_v f_y d}{V_s} = 4.85 \text{ in.}$$

where A_v is the area of 2 stirrup legs.

The web reinforcement was thus selected as

3 stirrups @ 4.5 in.

Beam 46:

This beam was also designed following the ACI - 63 Code, however it was assumed that the total shear has to be carried by web reinforcement. From the same equations as used for Beam 35 one obtains:

$$p_b = 0.0242$$

$$M_u = 8530 \text{ kip-in}$$

$$V_u = 109.5 \text{ kips}$$

Taking #4 stirrup-ties with f_y = 60 ksi, the required stirrup spacing is

$$s = 5.53 \text{ in.}$$

The web reinforcement was selected as #4 stirrups @ 6 in.

Beam 43:

For the design of this beam the special provisions for seismic design as stated in the ACI - 71 Code were taken into account; therefore, the limitation on the amount of longitudinal reinforcing steel is $p < 0.50\ p_b$. The contribution of the concrete to the shear resistance was neglected and the stirrup-ties were designed to resist the shear corresponding to the maximum moment possible in the beam. As was discussed in Section 2.3, this moment can be computed from

$$M_u = A'_s\ f_{max}\ (d-d')$$

With f_{max} equal to 97 ksi one obtains

$$M_u = 12500 \text{ kip-in}$$

$$V_u = 160.2 \text{ kips}$$

Taking #4 stirrups with f_y = 60 ksi, the required stirrup spacing is

$$s = 3.78 \text{ in.}$$

The web reinforcement was selected as

4 stirrups @ 3 in.

Some Significant Load Points:

a) Flexural Cracking Load:

$$M_{cr} = \frac{f_t I}{a}$$

where f_t = measured modulus of rupture

I = moment of inertia of transformed uncracked section

$a = \frac{h}{2} = 14.5$ in.

With the f_t values as listed in Table A6 the following values for M_{cr} were obtained:

Beam 35: M_{cr} = 1510 kip-in.

Beam 46: M_{cr} = 1690 kip-in.

Beam 43: M_{cr} = 1680 kip-in.

b) Working Stress Load:

The allowable working stresses are

for concrete in compression: $f_c = 0.45\ f'_c$

for deformed rebars: $f_s = 24000$ psi

Beam 35: The concrete strength governs, hence

$$M_{wl} = \frac{1}{2}\, 0.45\ f'_c\ kj\ bd^2$$

where $j = 1 - \frac{k}{3}$

and $k = \left[n^2\ (p+p')^2 + 2n\ (p+p'\frac{d}{d}) \right]^{\frac{1}{2}} - n\ (p+p')$

with $n = \frac{E_s}{E} = 8$ one obtains

$$M_{wl} = 2960 \text{ kip-in.}$$

Beam 46: Similarly to Beam 35 the concrete strength governs and the moment at working stress level is

$$M_{wl} = 3040 \text{ kip-in.}$$

Beam 43: Here the working stress level is attained first in the reinforcement, hence

$$M_{wl} = A_s f_s jd = 3160 \text{ kip-in.}$$

c) Diagonal Tension Cracking Load:

The specimens are assumed to exhibit diagonal tension cracks when the nominal shear stress v_c reaches the value

$$v_c = 1.9\sqrt{f'_c} + 2500\ p\ \frac{Vd}{M}$$

(Equation 11-4 in Reference 2)

Beam 35: $V_c = 49.5$ kips

Beam 46: $V_c = 50.5$ kips

Beam 43: $V_c = 56.0$ kips

EARTHQUAKE ENGINEERING RESEARCH CENTER REPORTS

EERC 67-1 "Feasibility Study Large-Scale Earthquake Simulator Facility", by J. Penzien, J. G. Bouwkamp, R. W. Clough, Dixon Rea - September 1967. (PB 187 905)*

EERC 68-1 Unassigned.

EERC 68-2 "Inelastic Behavior of Beam-to-Column Subassemblages Under Repeated Loading", by V. Bertero - April 1968. (PB 184 888)

EERC 68-3 "A Graphical Method for Solving the Wave Reflection-Refraction Problem", by H. D. McNiven and Y. Mengi - April 1968. (PB 187 943)

EERC 68-4 "Dynamic Properties of McKinley School Buildings", by D. Rea, J. G. Bouwkamp, R. W. Clough - November 1968. (PB 187 902)

EERC 68-5 "Characteristics of Rock Motions During Earthquakes", by H. B. Seed, I. M. Idriss, F. W. Kiefer - September 1968. (PB 188 338)

EERC 69-1 "Earthquake Engineering Research at Berkeley", January 1969. (PB 187 906)

EERC 69-2 "Nonlinear Seismic Response of Earth Structures", by M. Dibaj and J. Penzien - January 1969. (PB 187 904)

EERC 69-3 "Probabilistic Study of the Behavior of Structures During Earthquakes", by P. Ruiz and J. Penzien - March 1969. (PB 187 886)

EERC 69-4 "Numerical Solution of Boundary Value Problems in Structural Mechanics by Reduction to an Initial Value Formulation", by Nestor Distefano and Jaime Schujman - March 1969. (PB 187 942)

EERC 69-5 "Dynamic Programming and the Solution of the Biharmonic Equation", by Nestor Distefano - March 1969. (PB 187 941)

EERC 69-6 "Stochastic Analysis of Offshore Tower Structures", by Anil Kumar Malhotra and Joseph Penzien - May 1969. (PB 187 903)

EERC 69-7 "Rock Motion Accelerograms for High Magnitude Earthquakes", by H. B. Seed and I. M. Idriss - May 1969. (PB 187 940)

EERC 69-8 "Structural Dynamics Testing Facilities at the University of California, Berkeley", by R. M. Stephen, J. G. Bouwkamp, R. W. Clough and J. Penzien - August 1969. (PB 189 111)

EERC 69-9 "Seismic Response of Soil Deposits Underlain by Sloping Rock Boundaries", by Houshang Dezfulian and H. Bolton Seed - August 1969. (PB 189 114)

EERC 69-10 "Dynamic Stress Analysis of Axisymmetric Structures Under Arbitrary Loading", by Sukumar Ghosh and E. L. Wilson - September 1969. (PB 189 026)

EERC 69-11 "Seismic Behavior of Multistory Frames Designed by Different Philosophies", by James C. Anderson and V. Bertero - October 1969. (PB 190 662)

EERC 69-12 "Stiffness Degradation of Reinforced Concrete Structures Subjected to Reversed Actions", by V. Bertero, B. Bresler, Huey Ming Liao - December 1969. (PB 202 942)

EERC 69-13 "Response of Non-Uniform Soil Deposits to Traveling Seismic Waves", by H. Dezfulian and H. B. Seed - December 1969. (PB 191 023)

EERC 69-14 "Damping Capacity of a Model Steel Structure", by Dixon Rea, R. W. Clough and J. G. Bouwkamp - December 1969. (PB 190 663)

EERC 69-15 "Influence of Local Soil Conditions on Building Damage Potential During Earthquakes", by H. Bolton Seed and I. M. Idriss - December 1969. (PB 191 036)

EERC 69-16 "The Behavior of Sands Under Seismic Loading Conditions", by Marshall L. Silver and H. Bolton Seed - December 1969. (AD 714 982)

EERC 70-1 "Earthquake Response of Concrete Gravity Dams", by A. K. Chopra - December 1970. (AD 709 640)

EERC 70-2 "Relationships Between Soil Conditions and Building Damage in the Caracas Earthquake of July 29, 1967", by H. Bolton Seed, I. M. Idriss and H. Dezfulian - February 1970. (PB 195 762)

EERC 70-3 "Cyclic Loading of Full Size Steel Connections", by E. P. Popov and R. M. Stephen - July 1970.

EERC 70-4 "Seismic Analysis of the Charaima Building, Caraballeda, Venezuela", by Subcommittee of the SEAONC Research Committee, V. V. Bertero, Paul F. Fratessa, Stephen A. Mahin, Joseph H. Sexton, Alexander C. Scordelis, Edward L. Wilson, Loring A. Wyllie, H. Bolton Seed, Joseph Penzien, Chairman - August 1970. (PB 201 455)

EERC 70-5 "A Computer Program for Earthquake Analysis of Dams", by Anil K. Chopra - September 1970. (AD 723 994)

EERC 70-6 "The Propagation of Love Waves Across Non-Horizontally Layered Structures", by John Lysmer and Lawrence A. Drake - October 1970. (PB 197 896)

EERC 70-7 "Influence of Base Rock Characteristics on Ground Response", by John Lysmer, H. Bolton Seed and Per B. Schnabel - November 1970. (PB 197 897)

EERC 70-8 "Applicability of Laboratory Test Procedures for Measuring Soil Liquefaction Characteristics Under Cyclic Loading", by H. Bolton Seed and W. H. Peacock - November 1970. (PB 198 016)

EERC 70-9 "A Simplified Procedure for Evaluating Soil Liquefaction Potential", by H. Bolton Seed and I. M. Idriss - November 1970. (PB 198 009)

EERC 70-10 "Soil Moduli and Damping Factors for Dynamic Response Analysis", by H. Bolton Seed and I. M. Idriss - December 1970. (PB 197 869)

EERC 71-1 "Koyna Earthquake and the Performance of Koyna Dam", by Anil K. Chopra and P. Chakrabarti - April 1971. (AD 731 496)

EERC 71-2 "Preliminary In-Situ Measurements of Anelastic Absorption in Soils Using a Prototype Earthquake Simulator", by Roger D. Borcherdt and Peter W. Rodgers - April 1971. (PB 201 454)

EERC 71-3 "Static and Dynamic Analysis of Inelastic Frame Structures", by Frank L. Porter and Graham H. Powell - June 1971. (PB 210 135)

EERC 71-4 "Research Needs in Limit Design of Reinforced Concrete Structures", by V. Bertero - June 1971. (PB 202 943)

EERC 71-5 "Dynamic Behavior of a High-Rise Diagonally Braced Steel Building", by Dixon Rea, A. A. Shah and J. G. Bouwkamp - August 1971. (PB 203 584)

EERC 71-6 "Dynamic Stress Analysis of Porous Elastic Solids Saturated With Compressible Fluids", by Jamshid Ghaboussi and E. L. Wilson - August 1971.

EERC 71-7 "Inelastic Behavior of Steel Beam-to-Column Subassemblages", by Helmut Krawinkler, Vitelmo V. Bertero and Egor P. Popov - October 1971.

EERC 71-8 "Modification of Seismograph Records for Effects of Local Soil Conditions", by P. Schnabel, H. Bolton Seed and J. Lysmer - December 1971.

EERC 72-1 "Static and Earthquake Analysis of Three Dimensional Frame and Shear Wall Buildings", by E. L. Wilson and H. H. Dovey - May 1972.

EERC 72-2 "Accelerations in Rock For Earthquakes in the Western United States", by Per B. Schnabel and H. Bolton Seed - July 1972.

EERC 72-3 "Elastic-Plastic Earthquake Response of Soil-Building Systems", by Tadao Minami and J. Penzien - August 1972.

EERC 72-4 "Stochastic Inelastic Response of Offshore Towers to Strong Motion Earthquakes", by Maharaj K. Kaul and J. Penzien - August 1972.

EERC 72-5 "Cyclic Behavior of Three Reinforced Concrete Flexural Members With High Shear", by E. P. Popov, V. V. Bertero and H. Krawinkler - October 1972.

---

* Numbers in parentheses are Accession Numbers assigned by the National Technical Information Service. Copies of these reports may be ordered from National Technical Information Service, Springfield, Virginia 22151.